Separation of Interaction Wrench and Wind Disturbances from Wrench Observer in Fully-Actuated UAVs

Zulkarnaen

MSc Report

Committee:
Prof.dr.ir. G.J.M. Krijnen
R.A.M. Hashem, MSc
Dr.ir. J.B.C. Engelen
Prof.dr.ir. R.N.J. Veldhuis

January 2019

004RAM2019
Robotics and Mechatronics
EE-Math-CS
University of Twente
P.O. Box 217
7500 AE Enschede
The Netherlands

Summary

A UAV with physical interaction capabilities has potentials for scenarios where tool force control or contact inspection are required. This application requires the UAV to be able to control the interaction force while rejecting other disturbances, such as wind disturbances. Wrench observer provides an estimation of the disturbance wrench that is acting on the UAV; which includes interaction wrench, aerodynamic wrench, and model error.

This thesis is a preliminary study to implement blind signal separation (BSS) method, particularly independent component analysis (ICA), to separate interaction wrench and other disturbances—which includes wind disturbance—from the estimated disturbance of wrench observer.

Simulations and experiments of physical interaction on a fully-actuated hexarotor have been conducted. ICA has been applied to separate the observed disturbance of the acquired data. The result from the simulations shows that if the number of disturbances are limited, ICA could separate the observed disturbance. However, the real-world experiments show that the number of disturbances exceeds the number of the available measurement for ICA to perform well.

Contents

Summary iii

List of Acronyms vi

List of Notations vii

1 Introduction 1

1.1 Context . . . 1
1.2 Related Works . . . 3
1.3 Problem formulation . . . 4
1.4 Proposed Method . . . 5
1.5 Report Outline . . . 5

2 Background Theory 7

2.1 Wrench Observer on a UAV . . . 7
2.2 Interaction Model . . . 8
2.3 Independent Component Analysis . . . 9

3 Application of ICA for separating interaction wrench 13

3.1 Abstract . . . 13
3.2 Methodology . . . 13

4 Simulation 18

4.1 Simulation design . . . 18
4.2 Simulation results . . . 24

5 Experiments 39

5.1 Experiment designs . . . 39
5.2 Experiments Results . . . 44

6 Conclusions and Recommendations 51

6.1 Simulation Conclusions . . . 51
6.2 Experiments Conclusions . . . 51
6.3 Overall Conclusions . . . 51
6.4 Recommendations . . . 51

Bibliography 53

List of Acronyms

BLDC Brushless direct current

BSS Blind signal separation

DFD Data flow diagram

FFT Fast Fourier Transform

GUI Graphical user interface

IC(s) Independent component(s)

ICA Independent component analysis

IMU Inertial measurement unit

MEMS Micro-electromechanical systems

NDT Non-destructive testing

RMSE Root mean square error

RMS Root mean square

ROS Robot operating system

UAV Unmanned aerial vehicle

pdf Probability density function

List of Notations

Below are the summary of the notations which are used in this thesis.

ψ_a	Right-handed reference frame with label a.
p_a^b	Position of origin of ψ_a expressed in ψ_b.
R_a^b	Rotation matrix of ψ_a to ψ_b.
H_a^b	Homogeneous transformation matrix from ψ_a to ψ_b: $H_a^b = \begin{pmatrix} R_a^b & p_a^b \\ 0_3 & 1 \end{pmatrix} \in SE(3)$
v	Linear velocity of the body attached to frame ψ_a with respect to the body attached to frame ψ_b expressed in frame ψ_c
ω	Angular velocity of the body attached to frame ψ_a with respect to the body attached to frame ψ_b expressed in frame ψ_c
$T_a^{c,b}$	Twist of the body attached to frame ψ_a with respect to the body attached to frame ψ_b expressed in frame ψ_c $T_a^{c,b} = \begin{pmatrix} \omega_a^{c,b} \\ v_a^{c,b} \end{pmatrix} \in SE(3)$
F^a	Force expressed in ψ_a.
τ^a	Torque expressed in ψ_a.
W^a	Wrench expressed in ψ_a. $W^a = \begin{pmatrix} \tau^a & F^a \end{pmatrix} \in SE(3)$
$\mathbf{A}$	ICA mixing matrix.
$\mathbf{W}$	ICA unmixing matrix. $\mathbf{W} = \mathbf{A^{-1}}$.
$\mathcal{I}$	Inertia tensor of UAV expressed in ψ_B
$\mathcal{P}^B$	Moment of body B expressed in ψ_I
σ	Standard deviation

The following frame are used in this thesis:

ψ_B	Body frame.
ψ_{ee}	End-effector frame.
ψ_0	World frame.
ψ_s	Sensor frame.
ψ_d	Desired position frame.

1 Introduction

1.1 Context

Unmanned Aerial Vehicles (UAVs) are becoming increasingly popular. Its advancement is mutually supportive to the advancement of technologies of material (e.g., carbon fibers), sensors (e.g., Micro-electromechanical systems (MEMS)), actuator (e.g., brushless direct current (BLDC) motor), onboard computing and communication, and algorithm (e.g., sensor fusions and control) [1] which supports it. The diversity of sector which are interested in the research also drives UAV implementation to various fields such as delivery, disaster response, infrastructure maintenance management, surveying, agriculture, forestry, and fisheries [2]. In those fields, UAVs commonly served as an “eyes in the sky” or a “flying cargo transporter” where they are designed and optimized for free flight. In recent year, research of UAVs with the capability of physical interaction with the environment has become a new focus.

There are a lot of potential applications for a UAVs which require maintaining a certain level of contact with an object such as contact inspection—some example scenarios in the industrial and construction sector include crack detection, weld inspection, corrosion detection, coating thickness detection, and checking material properties. Those scenarios require the sensor which positioned by the UAV to maintain its contact. Another potential scenario would be human and aerial-robot interaction. These potential applications lead to more research towards UAVs with physical interaction [3].

This potentials also led researchers to investigate various novel designs which are suitable for physical interaction task. Nowadays, most multi-rotor UAVs are optimized for free flight, where all of its rotors are pointed upwards. It results in an underactuated UAV where there is a coupling between the translational and rotational dynamics of the UAV. This coupling limits the UAVs performing complex physical interaction task. One of the design solution—which also used in this project, see Figure 1.1—is to tilt the propellers of a hexarotor by a fixed angle about one axis. This solution solved the underactuation problem with some drawbacks. First, it reduces the power delivered by the propellers—a trade-off for a fully-actuated system. Second, this design suffers from internal aerodynamic interferences that are complicated to be modeled and cause time-varying disturbances to the motion control system.

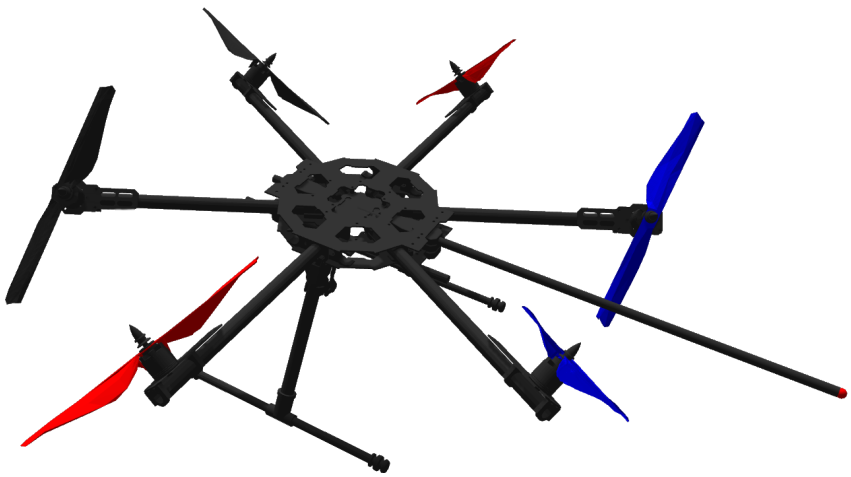

Figure 1.1: BetaX, a fully actuated hexarotor with an end-effector attached

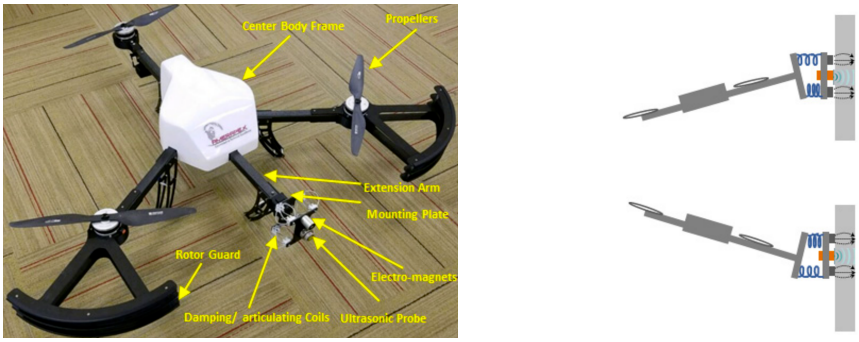

(a) The UAV and its components **(b)** Scenarios during wall-sticking

Figure 1.2: Wall-sticking UAV for Non-Destructive Ultrasonic and Corrosion Testing [4]

Regarding solution for controlling contact with a surface, there are several solutions. The first solution would be to use an open-loop force control. An example of open-loop force control can be seen in a tri-copter that is attached with a Non-Destructive Testing (NDT) measurement units on its end effector in Figure 1.2. Those measurement units require contact with the surface it measures. To maintain contact with the surface structure, the UAV rely on the forward force from propellers, with an addition of two electro-magnet coil which is added to the end effector to make sure a proper contact between the measurement unit and the surface.

A better solution would be to use a closed-loop force control. In principle, the disturbance could be measured or estimated [5]. The second solution would be to implements a closed-loop force control with feedback acquired from a torque sensor at UAV end-effector. From the control perspective both the first and the second solutions are relatively easy to implement, but not without problem. Both solutions added complexity to the mechanical component, less flexibility of the direction of the interaction, and adding both payload and electrical load to the already limited resource UAV.

The third solution is to estimate the force feedback using available information. There are two approaches to estimate the interaction wrench. First, is to estimate the interaction using contact-impedance estimation. This method is suitable for UAV with non-rigid end-effector as shown in [6]. The other method is called wrench observer [1]. It uses UAV's rigid body model, its pose, and control input to estimate disturbance wrench (force + torque). Which means, it estimates wrench that is not included in the model. This method is considered to be simpler to implement since it does not need additional complexity to the mechanical component and flexibility in the direction of disturbance sources.

However, since wrench observer estimates any wrench that is not part of the model which include aerodynamic disturbances and modeling error, it could not distinguish which one is which. Ideally, we want to treat the interaction disturbance and aerodynamic disturbance differently. Interaction disturbance could be used for feedback in force control, while the other disturbance could be rejected in the position control in a feedforward manner. An example block diagram for UAV which treats the disturbance separately can be seen in figure 1.3. In the block diagram, a disturbance separation block is added to separate observed disturbance into interaction wrench and other disturbance.

By having disturbance separation capabilities in a UAV system which uses wrench observer, it is possible to perform an interaction with a surface structure in a closed-loop force control manner, while also having the possibility of rejecting other disturbances.

[1] This method will further be discussed in chapter 2.

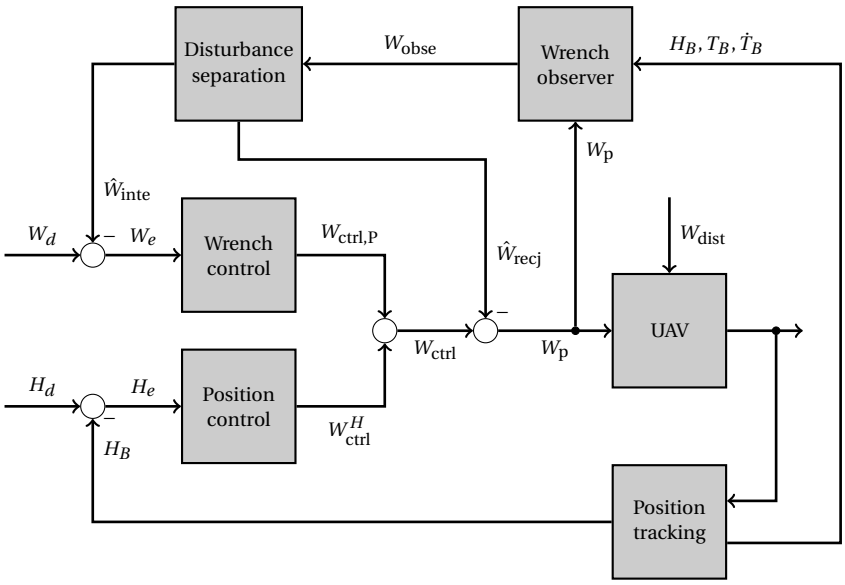

Figure 1.3: UAV controller with wrench observer equipped adapted from [7]

1.2 Related Works

The author in [5] has done extensive research regarding wrench observer, collision detection, and interaction control for a UAV. A hybrid wrench observer was proposed in his work in [8] where he combined a momentum-based estimation—which is suitable to estimate external torques—and acceleration-based estimation—which is suitable to estimate external forces.

Later on, he extended this work in [9] by adding an aerodynamic model to the wrench observer for metric wind estimation and collision detection. First of all, it generalizes the mixing matrix[2] by adding incorporating true airspeed to the model. He also added drag model of the UAV. The aerodynamic drag wrench is a function of true airspeed multiplied with the drag coefficient of the UAV.

Using the framework mentioned above, he proposed two methods to separate between aerodynamic and contact force. The first one is filter-banks where he uses spectrum analysis of external wrench during flight. He isolated the frequency of the corresponding source and designed an appropriate filter. However, quasistatic contact forces cannot be distinguished by this method. The next one is model checking, where it a uses an estimation of wind velocity and the previously motioned drag coefficient to estimate aerodynamic disturbance. The residual wrench will then contain contact wrench and modeling errors.

A study of contact impedance estimation for robotic systems was done in [10]. It compares a classical *Kelvin-Voigt* model of contact which uses a linear model of spring and damper and *Hunt-Crossley* model of contact which uses a nonlinear model of it. The contact force is a function of penetration depth. A contact between two rigid objects would be hard to estimate unless a high precision position measurement is used. The author in [6] explores the implementation of the previous model on a UAV for a contact inspection. He achieved that by using impedance control and a non-rigid special manipulator.

Signal separation, which includes disturbance, is considered as a classical problem in the field of signal processing. The problem of separating signal without prior knowledge of the system, is called blind signal separation (BSS) problem. It is called “blind” because the technique tries to estimate the “source” of the signal by using only the measured signal. There are sev-

[2] In this context, a mixing matrix is a matrix which relates between each propellers’ angular velocity and the total thrust wrench generated.

eral technique which related to BSS including principal component analysis (PCA) [11] and the more recent Independent component analysis (ICA) [12]. The latter technique is thoroughly explained in [13].

1.3 Problem formulation

To formulate the problem, we will start from the component of the disturbance which wrench observer estimate. The output of wrench observer W_{obse} is an estimation to the disturbance wrench in the system W_{dist}. The disturbance in the system can be expressed as

$$W_{\text{dist}} = W_{\text{inte}} + W_{\text{aero}} + W_{\text{errm}} \tag{1.1}$$

which is the sum of interaction disturbance W_{inte}, aerodynamic disturbance W_{inte}, and modeling error W_{errm}. A wrench $W = \begin{bmatrix} \tau \\ F \end{bmatrix}$ is a vector which combines torque τ and force F. Focusing on the force component of the disturbance, equation 1.1 can be expressed as

$$F_{\text{dist}} = F_{\text{inte}} + F_{\text{aero}} + F_{\text{errm}}. \tag{1.2}$$

Assuming there is no modelling error and using vector-matrix notation, the previous equation can be rewritten as

$$F_{\text{dist}} = \begin{bmatrix} F_{\text{x,dist}} \\ F_{\text{y,dist}} \\ F_{\text{z,dist}} \end{bmatrix} = \mathbf{A}_I \cdot \begin{bmatrix} F_{\text{x,inte}} \\ F_{\text{y,inte}} \\ F_{\text{z,inte}} \\ F_{\text{x,aero}} \\ F_{\text{y,aero}} \\ F_{\text{z,aero}} \end{bmatrix}, \tag{1.3}$$

with $\mathbf{A}_I$ is a 3 by 6 mixing matrix which relates the components of disturbances, interaction wrench and aerodynamic disturbance, to the total disturbance. In equation 1.3 the mixing matrix is defined as two identity matrix

$$\mathbf{A}_I = \begin{bmatrix} I & I \end{bmatrix}. \tag{1.4}$$

For an unknown source of disturbance, equation 1.3 can be generalized as

$$\begin{bmatrix} F_{\text{x,dist}} \\ F_{\text{y,dist}} \\ F_{\text{z,dist}} \end{bmatrix} = \mathbf{A} \cdot \begin{bmatrix} F_{\text{comp,1}} \\ \vdots \\ F_{\text{comp,6}} \end{bmatrix}, \tag{1.5}$$

with A as a generalized mixing matrix which relates the disturbance components to the total disturbance. Now the problem can be expressed as a blind signal separation (BSS) problem with $\mathbf{F}_{\text{dist}}$ considered as the measurement from "microphone" and $\mathbf{F}_{\text{comp}}$ considered as "source".

$$\begin{aligned} \mathbf{F}_{\text{dist}} &= \mathbf{A} \cdot \mathbf{F}_{\text{comp}} \\ \mathbf{x} &= \mathbf{A} \cdot \mathbf{s}. \end{aligned} \tag{1.6}$$

The same formulation could also be expressed for the torque component τ of the disturbance wrench.

This thesis a preliminary study into the topic of implementing applying BSS on disturbance separation problem. Therefore, this thesis is only focusing on the force component of the wrench disturbance. Moreover, to have an invertible square mixing matrix, a matching dimension between the number of measurement from the "microphone" and the number of "source" is required. Thus, it is assumed that there are only three source of disturbances.

Using the assumptions that is provided above, the equation 1.5 is re-expressed with three disturbance component as

$$\begin{bmatrix} F_{\text{x,dist}} \\ F_{\text{y,dist}} \\ F_{\text{z,dist}} \end{bmatrix} = \mathbf{A} \cdot \begin{bmatrix} F_{\text{comp,1}} \\ F_{\text{comp,2}} \\ F_{\text{comp,3}} \end{bmatrix} \tag{1.7}$$

with $\mathbf{A}$ as a 3 by 3 mixing matrix. Provided the columns of mixing matrix is unique, an unmixing matrix $\mathbf{W}$ which is the defined as $\mathbf{A}^{-1}$ can be determined used to obtain the component of the disturbances using the following equation

$$\begin{bmatrix} F_{\text{comp,1}} \\ F_{\text{comp,2}} \\ F_{\text{comp,3}} \end{bmatrix} = \mathbf{W} \cdot \begin{bmatrix} F_{\text{x,dist}} \\ F_{\text{y,dist}} \\ F_{\text{z,dist}} \end{bmatrix}. \tag{1.8}$$

With the assumption that there are only two components of the interaction wrench—which are friction wrench due to movement in one axis[3] along the surface and contact wrench from pushing the surface of the structure—there is one dimension which can be occupied with aerodynamic disturbance or modelling error.

Provided that the assumption above is fulfilled, then it is possible to separate the disturbance into interaction wrench and other disturbances and treat each component accordingly.

> The goal of this thesis is to come up with a method to separate interaction forces F_{inte} and other disturbances including aerodynamic disturbance from wrench observer on a fully-actuated UAV and test its performance.

1.4 Proposed Method

In this thesis, I propose to use blind signal separation (BSS) technique, particularly independent component analysis (ICA), to separate the interaction force and other disturbances from observed disturbance. The proposed method can be divided into three states.

First, the UAV is going hover in the near the surface of the structures. During this state the UAV will obtain prior knowledge of the observed disturbance.

Next, the UAV perform a calibration maneuver which involve some movement along the surface of the structure. The data that is acquired during the calibration state is fitted into ICA to generate an unmixing matrix. Using the unmixing matrix, the observed disturbance from the first state and the second state is transformed into independent components (ICs).

With the assumption that the ICs independent from each other, then an IC that is not related to interaction wrench could be identified by finding similar IC between both states. To cancel the effect of the related IC, a filtered mixing-matrix is generated. The matrix is generated by inverting the unmixing matrix and canceling the column which is not related to interaction wrench.

The interaction force could then be estimated by using the filtered mixing-matrix. On the other hand, other disturbance can be estimated by subtracting the observed disturbance with the estimated disturbance. This proposed method would be further explained in chapter 3.

1.5 Report Outline

This report is presented in six chapters. Chapter 1 is the introduction which explains the background and objectives of this research. Chapter 2 presents the background theory related to

[3] The movement is limited to one axis to reduce the dimension of the source, so that it matched with the dimension of the measurement.

this project. Chapter 3 will explain the proposed method in detail. Chapter 4 will explain the simulations and its result, while in chapter 5 will explain the experiments and its results. Finally, conclusions are drawn, and some further research options are given in Chapter 6.

2 Background Theory

In this chapter, background theory which is related to the thesis will be presented. This chapter consists of three sections, wrench observer on a UAV, contact model, and independent component analysis.

2.1 Wrench Observer on a UAV

The wrench observer used in this thesis is based part of the work in [14] where an observer-based wrench/impedance controller for a fully actuated hexarotor is implemented. It uses wrench observer to estimate the interaction wrench without the use of a force/torque sensor. Another work that is working on wrench observer are [8] which present a unified framework for external wrench estimation. It uses a different approach from the former reference. The former approach assumes the wrench observer have the complete data of UAV which include pose (orientation and position), twist (linear velocity and angular velocity), and acceleration (linear acceleration and angular acceleration). This assumption is valid for the simulations and the experiments which are performed in this thesis.

A UAV control system could be equipped with a wrench observer to reject disturbances in a feedforward manner. It increases robustness against modeling error and other disturbances. The output of wrench observer can be used as compensation to the control in a feedforward manner.

Newton's second law $F = ma$ can be generalized to a rigid body as

$$\dot{\mathcal{P}}^B = ad^{\top}_{T^{B,I}_B}\mathcal{P}^B + W^B, \tag{2.1}$$

with $\mathcal{P}^B = \mathcal{I}T^{B,I}_B$ as the moment of UAV body expressed in the inertial frame. A generalized moment is denoted as $\mathcal{P}$, generalized inertia tensor is denoted as $\mathcal{I}$, and twist which is a vector of translation velocity and angular velocity $T = \begin{bmatrix}\omega \\ v\end{bmatrix}$. Adjoint time derivative is denoted as ad_T.

The motion equations of the UAV is given by [14]

$$\dot{\mathcal{P}}^B = ad^{\top}_{T^{B,I}_B}\mathcal{P}^B + W^B_g + W^B_p + W^B_{dist}, \tag{2.2}$$

There are three wrenches which are acting on the UAV: rigid body dynamics $ad^{\top}_{T^{B,I}_B}\mathcal{P}^B$, gravity W^B_g, propeller thrust W^B_p, and disturbances W_dist^B. For simplicity, the previous equation will be rewritten as

$$\dot{\mathcal{P}} = f(\mathcal{P}, W_p) + W_{dist}, \tag{2.3}$$

with $f(\cdot)$ as a function with inputs of generalized momentum $\mathcal{P}$ and input wrench from the propellers W_p, plus the remaining of the terms in equation 2.2 minus disturbance wrench W_{dist}. An estimation of the disturbance is defined by

$$\hat{W}_{dist} = K_0(\mathcal{P} - \delta), \tag{2.4}$$

$$\dot{\delta} = f(\mathcal{P}, W_p) + K_0(\mathcal{P} - \hat{\delta}), \tag{2.5}$$

with $\delta \in \mathbb{R}$ as an auxiliary variable of the observer, and $K_0 \in \mathbb{R}$ as a positive diagonal matrix of gains. The disturbance estimation error is defined as $e_{dist} = \hat{W}_{dist} - W_{dist}$ with disturbance error dynamic

$$\dot{e}_{dist} = -K_0 e_{dist} - \dot{W}_{dist}. \tag{2.6}$$

The estimated disturbance will converge to actual value with rate specified by gain K_0. From equation 2.3 it can be seen that disturbance W_{dist} is any wrench that is not modeled in the equation. It means disturbance includes aerodynamic disturbance, interaction disturbance, and modeling error

$$W^B_{dist} = W^B_{aero} + W^B_{inte} + W^B_{merr}. \tag{2.7}$$

An example of how wrench observer is integrated into a system can be seen in Figure 1.3. There, a closed-loop system controls the position of the UAV using the error H_e between the desired position H_d and the actual body position H_B. Using position error, the gains in position control block results in the wrench W_{ctrl} that is going is going to be sent to the propeller. The disturbance—in the form of aerodynamic disturbance, interaction disturbance, and modeling error—are inflicted to the rigid body of the UAV.

For a UAV to be able to maintain contact, it needs to be able to distinguish between disturbance that needs to be rejected—in this case, aerodynamic disturbance and modeling error—and interaction disturbance that could be used to control the interaction force with the object the UAV is interacting with. Another thing that has to be noted is if a UAV intend to interact with a UAV with the disturbance rejection activated the behavior of the UAV could be erratic.

2.2 Interaction Model

Due to the interest in controlling the interaction of a robotic system with its environments, there have been several studies in modeling the interaction. Some of the studies for robotic interactions includes [10], including one that is specifically related to UAV [6].

For 1-D contact, the simplest method to model the interaction is to use linear spring and viscous damper model, known as Kelvin-Voigt. It considers the contact material as an ideal viscoelastic material.The equation is described as follow

$$F(t) = \begin{cases} Kx(t) + B\dot{x}(t), & x \geq 0 \\ 0 & x < 0 \end{cases}, \tag{2.8}$$

with x represent the depth of probe's penetration, $\dot{x}$ represent the velocity of the probe, and—K and B are the elastic and viscous parameter of the contact. However, when the penetration is small, the dominant component would be the damping term, which causes inconsistencies.

The problem can be overcome by considering that the viscous force is made dependent on the penetration depth as proposed by Hunt-Crossley with the following equation

$$F(t) = \begin{cases} Kx^n(t) + \lambda x^n(t) B\dot{x}(t), & x \geq 0 \\ 0 & x < 0 \end{cases} \tag{2.9}$$

Penetration depth and its velocity against a surface combined with the interaction model can be used to estimate interaction force. However, since the penetration depth and velocity of a rigid rigid to rigid contact is relatively small, it is not feasible to implement it on UAV with a rigid end-effector.

2.3 Independent Component Analysis

Independent component analysis (ICA) is a method of finding underlying factors or components from multivariate (multidimensional) statistical data [13]. It transforms the data so that its essentials structure is made more visible or accessible. The technique of ICA, although not yet the name, introduced in the early 1980s in neurophysiological setting to infer position and velocity signals of muscle signal—e.g. $s_1(t), s_2(t)$—from the measured responses—e.g. $x_1(1), x_2(t)$.

Currently, ICA becomes an exciting topic both in the field of neural networking—especially unsupervised learning—and more generally in advanced statistics and signal processing. Its applications grow into the field of biomedical signal processing, audio signal separation, telecommunications, fault diagnosis, feature extraction, financial time series analysis, and data mining.

2.3.1 Blind Signal Separation

In many cases, the measurements are given as a set of parallel signals or time series. However, the measurements do not reflect the thing that is intended to be measured, i.e., the sources. Instead, it is a combination of the sources mixed with an unknown mixture. This kind of problem is referred to as blind signal separation (BSS) problem. The goal which BSS try to solve is to estimate the source signals and how it is mixed, provided with only the recorded measurements.

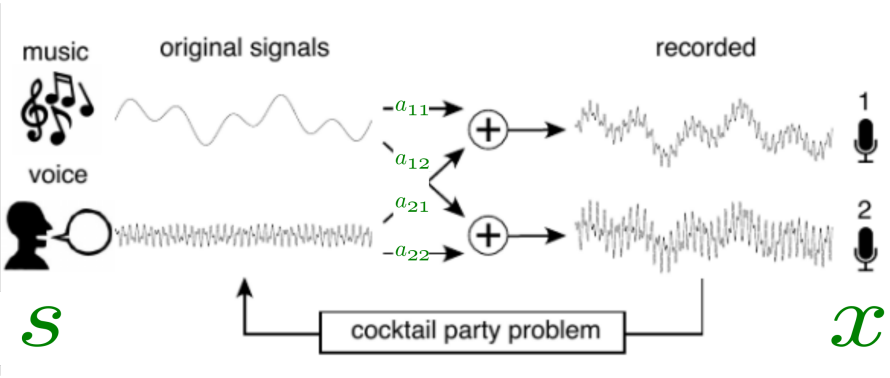

Figure 2.1: Cocktail party problem [12]

Consider a cocktail party situation in Figure 2.1. There are two sources of sounds in the room, the voice from a person and the sound of the music which we denote by $s_1(t)$ and $s_2(t)$, with $s1$ and s_2 the amplitudes and t the time index. Two microphones are also positioned in the room which which gives two recorded time signals, which we denote by $x_1(t)$ and $x_2(t)$.

Each of these recorded signals is a weighted sum of the sounds emitted by the two sources. For the time being, we ignore time delay or other extra factors to simplify the model. Then we could express this as a linear equation

$$\begin{aligned} x_1(t) &= a_{11}s_1(t) + a_{12}s_2(t) \\ x_2(t) &= a_{21}s_1(t) + a_{22}s_2(t) \end{aligned}, \tag{2.10}$$

where the a_{ij} with $i, j = 1,2$ are parameters which depend on the relative position between the microphones and the sound sources. It would be useful if $s_j(t)$ could be estimated using only the recorded signals $x_i(t)$. This kind of problem is well known as the cocktail-party problem.

For convenience, the previous equation could be generalized into vector-matrix notation by denoting $\mathbf{x}$ as a vector whose elements are mixtures of $x_1, \ldots, x_n$ and likewise $\mathbf{x}$ as a vector whose elements are mixtures of $s_1, \ldots, x_n$. Using this notation, the previous equation could be expressed as

$$\mathbf{x} = \mathbf{A} \cdot \mathbf{s} \tag{2.11}$$

An estimation of **s** can be denoted as **y** by re-expressing the previous equation as

$$\begin{aligned} y_1(t) &= w_{11}x_1(t) + w_{12}x_2(t) \\ y_2(t) &= w_{21}x_1(t) + w_{22}x_2(t) \end{aligned}. \tag{2.12}$$

which can also be re-expressed in vector-matrix equation as

$$\mathbf{y} = \mathbf{W} \cdot \mathbf{x} \tag{2.13}$$

with **W** as an unmixing matrix with components consists of w_{ij}.

Now the problem can be formulated as, provided the observed signal of **x**, we want to estimate the unmixing matrix **W** such that the estimated source **y** is equal to the sources **s**.

2.3.2 Definition of ICA

Independent component analysis was initially developed to deal with problems that are closely related to the cocktail-party problems. A basic ICA model can be defined using statistical "latent variables" model as a generative model of n observed random variables $x_1, \ldots, x_n$ which are modeled as linear combinations of n random variables $s_1, \ldots, s_n$

$$x_i = a_{i1}s_1 + \cdots + a_{in}s_n, \qquad \text{for all } i = 1, \ldots n \tag{2.14}$$

where $a_{ij}, i, j = 1, \ldots n$ are some real coefficients, with s_i defined as statistically mutually independent. In this context, a generative model means that the observed data are generated by the process of mixing the latent independent component s_j (often abbreviated as IC) which cannot be observed directly. This equation can be generalized using vector-matrix notation as equation 2.11.

Using equation 2.13 as a reference, Independent component analysis (ICA) can be defined as finding a linear transformation **W**, such that components of **y** are statistically as independent as possible. Provided that the sources are not gaussian[1], the unmixing matrix **W** could be determined such that **y** is equal to **s**.

A basic ICA model also makes some additional assumptions:

1. The time component t from the equation is dropped because we assume that each mixture of x_i and s_j is a random variable, instead of a proper time series.
2. The time delay which might occur during the mixing is neglected which makes the basic model called instantaneous mixing model.
3. Additional noise is neglected in the basic model.
4. The number of ICs and observed mixtures is assumed to be equal.
5. The mixing is assumed to be linear.

2.3.3 Restrictions in ICA

The basic ICA model can be estimated provided the following restrictions are followed:

1. The independent components are assumed statistically independent.

   This is the basic principles of ICA. Random variables of $y_1, \ldots, y_n$ are said to be independent if information on the value of y_i does not give information on the value of y_j for $j \neq i$. It can also be defined using probability density as

   $$p(y_1, \ldots, y_n) = p_1(y_1) \ldots p_n(y_n), \tag{2.15}$$

[1] It is still possible to estimate the model with one gaussian source [13, pg. 163]

with $p(y_1,\ldots,y_n)$ as joint probability density function (pdf) of y_i and $p_i(y_i)$ as the marginal pdf of y_i.

It will be explained in more detain in the next subsection.

2. The independent components must have nongaussian distribution.

   ICA would not be able to separate gaussian component from each other. Therefore, in the case of just one gaussian component, ICA would still be able to estimate the model

3. For simplicity, the unknown mixing matrix is square.

   In this case, the number of ICs are equal to the number of observed mixtures. This restriction is provided to simplify the estimation; however, it is possible to have a non-square matrix. Another assumption is that the mixing matrix is invertible. If it is not invertible, then there are redundant mixtures that could be omitted, then the matrix would not be square.

2.3.4 Ambiguities of ICA

Some ambiguities hold for ICA model

1. We cannot determine the variance (energies) of the independent component.

   Considering equation 2.11, any scalar that is multiplied in one of the sources s_i could always be canceled in the corresponding column $\mathbf{a_i}$ of $\mathbf{A}$.

2. We cannot determine the order of the independent component.

   With both $\mathbf{s}$ and $\mathbf{A}$ being unknown, the order of the component can be freely changed.

2.3.5 Statistical independence

In this section, the term of statistical independence will be explained. For simplicity, in the case of two different scalar random variables x and y. The random variable x independent of y means knowing the value y does not give any information on the value of x and vice versa. Examples of such independent random variables are the value of a dice thrown and a coin tossed, or speech signal and background noise.

Mathematically, statistical independence is defined in terms of probability p, with random variables x and y are said to be independent if and only if

$$p_{x,y}(x,y) = p_x(x)\,p_y(y). \tag{2.16}$$

In words, the previous equation would be described as, the joint density $p_{x,y}(x,y)$ of x and y must factorize into the product of their marginal densities $p_x(x)$ and $p_y(y)$.

Independent random variables satisfy the fundamental property of uncorrelatedness between $g(x)$ and $h(y)$

$$E\{g(x)h(y)\} = E\{g(x)\}\,E\{h(y)\} \tag{2.17}$$

where $g(x)$ and $h(y)$ could be any integrable functions of x and y respectively. $E\{z\}$ is the expectation of z. This property of shows that statistical independence is a much stronger property of uncorrelatedness compared to the simple uncorrelatedness of

$$E\{xy\} = E\{x\}\,E\{y\} \tag{2.18}$$

which leads to better performance in separation.

2.3.6 Estimating ICA model

The principal of ICA method is based on the central limit theorem, which says that the distribution of a sum of independent random variables tends toward a gaussian distribution.

Considering the previous mixing equation of

$$\mathbf{x} = \mathbf{A} \cdot \mathbf{s}, \tag{2.19}$$

then based on the central limit theorem $\mathbf{x}$ is more gaussian than $\mathbf{s}$. The same principal could be applied to estimate the source $\mathbf{s}$ using

$$\mathbf{y} = \mathbf{W} \cdot \mathbf{x}. \tag{2.20}$$

The fundamental idea of the estimation is $\mathbf{y}$ is less gaussian when it is closer to the value of the actual source $\mathbf{s}$.

There are various implementations of ICA based on how the separation is calculated and how the nongaussianity is measured. One of the methods to estimate the ICA model is FastICA which uses Newton's approximation on negentropy to measure nongaussianity.

Negentropy is based on the information-theoretic quantity of differential entropy, or simply entropy. It is related to the information that the observation of the variable gives. The more "random" the variable is, the larger its entropy. The entropy H of random vector $\mathbf{y}$ with given density $p_y(n)$ is defined as

$$H(\mathbf{y}) = -\int p_y(n) \log p_y(n) \mathrm{d}n. \tag{2.21}$$

Using the equation, a gaussian variable would have the largest entropy. To measure nongaussianity, the previous equation could be normalized as negentropy J

$$J(\mathbf{y}) = H(\mathbf{y}_{gauss}) - H(\mathbf{y}). \tag{2.22}$$

Using this property, negentropy would be zero only if $\mathbf{y}$ has a gaussian distribution; otherwise it would have a positive value.

3 Application of ICA for separating interaction wrench

This chapter will discuss the proposed technique to separate interaction wrench from observed disturbance. The chapter will be started with the abstraction of UAV operation states during the interaction and followed with the proposed methodology to separate the observed wrench.

3.1 Abstract

Consider the UAV operation states during the interaction with a structure as depicted in Figure 3.1. In the state-1, the UAV is away from the structure that it is going to interact with. Assuming that there is no modeling error, $F^B_{merr} = 0$, and no external wind, $F^B_{aero} = 0$, then the disturbance F^B_{dist} during this state would be zero.

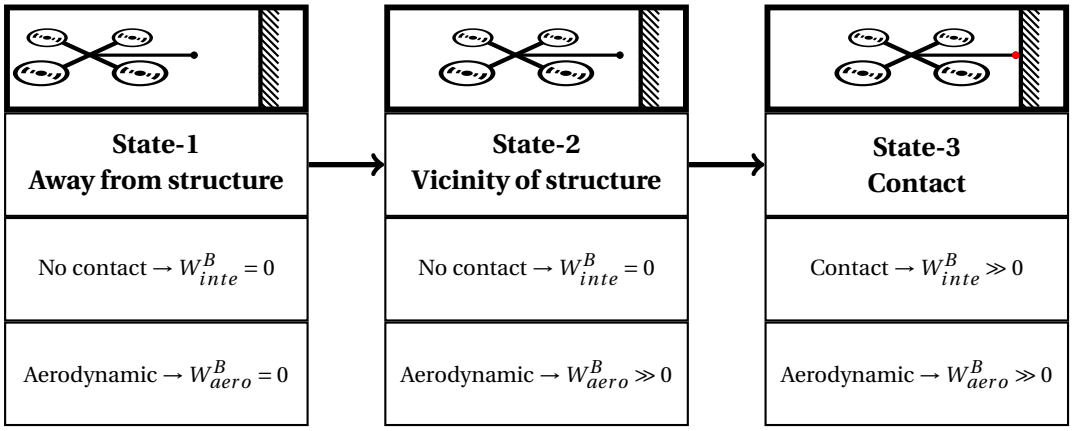

Figure 3.1: UAV interaction operation states

In state-2, the UAV is in the vicinity of the structure. In this state, especially with the case of a fully-actuated UAV, it is assumed that the aerodynamic disturbance is pretty significant $F^B_{aero} \gg 0$ due to the wind of the propeller bouncing off the surface. Thus, the observed disturbance would only consist of the aerodynamic disturbance.

In state-3, the UAV come into contact with the surface of the structure. In this state, the disturbance is the combination of aerodynamic disturbance and interaction disturbance.

3.2 Methodology

In this section, the methodology that is used in this thesis will be explained in detail. First, the operation state of the separation will be explained. Then, some detail regarding the configuration that is used will be explained.

3.2.1 Separation states

The basic idea of the proposed separation method is to use the comparison of the observed disturbance F^B_{obse} between state-2 and state-3 to provide more accurate estimates of interaction wrench F^B_{inte}. The method is separated into three states of a modified version of the UAV interaction operation states in Figure 3.1.

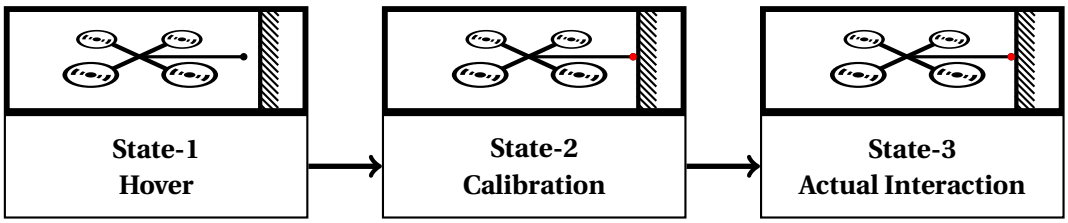

Figure 3.2: Separation states

Figure 3.2 shows the three states of the separation process. To simplify the notation, unless otherwise stated, the wrench in the following report is expressed in the UAV body frame. The process in each state are explained below:

state-1 (hover) is when the UAV is hovering in the vicinity of the surface of the structure that it is going to interact with. In this state, the observed disturbance would be sampled. It changes to the next state triggered by a collision with the surface. The time series of the observed disturbance during these states will be denoted as $F_{\text{obse}}^{\text{prio}}$.

state-2 (calibration) is when the UAV perform a calibration specified movement along the surface of the structure. The movement is set to be minimum, to minimize the chance of damage that is caused by uncontrolled interaction. Using the sampled observed disturbance during this state, the separation process does the following steps:

1. Perform ICA on the observed disturbance $F_{\text{obse}}^{\text{cali}}$ to generate an unmixing matrix $\mathbf{W}$.
2. Transform the observed disturbance from state-1 and state-2 to independent components using the generated unmixing matrix.

$$\begin{aligned} S^{\text{prio}} &= \mathbf{W} \cdot F_{\text{obse}}^{\text{prio}} \\ S^{\text{cali}} &= \mathbf{W} \cdot F_{\text{obse}}^{\text{prio}} \end{aligned} \tag{3.1}$$

3. Determine which independent component (IC) that is similar in state-1 and state-2 using frequency analysis. To find similar IC, a method that is "phase independent" is required. The proposed method to determine the similar IC are:
   (a) Transform the ICs of both S^{prio} and S^{cali} to the frequency domain using Fast Fourier Transform (FFT).
   (b) In the frequency domain, the root mean square (RMS) of difference between the IC of the same index between state S^{prio} and S^{cali} are calculated and determined as similarity coefficient.
   (c) The IC with the smallest similarity coefficient is considered to be a similar component.
4. Generate a mixing matrix with using the inverse of the unmixing matrix with the column which is similar in both state-1 ,and state-2 canceled (set the corresponding column to zero) $\mathbf{A}_{\text{filt}}$.

state-3 (actual interaction) consists of the following steps:

- Estimate interaction wrench $\hat{F}_{\text{inte}}$ by canceling the component which is related to the aerodynamic disturbance. It is achieved by transforming observed disturbance $F_{\text{obse}}^{\text{inte}}$ using both unmixing matrix $\mathbf{W}$ and filtered mixing-matrix $\mathbf{A}_{\text{filt}}$.

$$\hat{F}_{\text{inte}} = \mathbf{W} \cdot \mathbf{A}_{\text{filt}} \cdot F_{\text{obse}} \tag{3.2}$$

- Lastly, the residual of the observed wrench can be estimated as aerodynamic disturbance.

$$\hat{F}_{\text{aero}} = F_{\text{obse}} - \hat{F}_{\text{inte}} \tag{3.3}$$

A detailed block diagram of disturbance separation which complements the block diagram in Chapter 2 is presented in figure 3.3. As shown in the diagram, the disturbance separation block diagram performs the separation using the signal from the wrench observer to estimate both interaction wrench and aerodynamic disturbance. Figure 3.4 shows a more comprehensive separation process as a data flow diagram (DFD). The data flows from the top to the bottom with the data from state-1, followed by state-2, and state-3. The outcome of the DFD is located at the bottom right of the diagram.

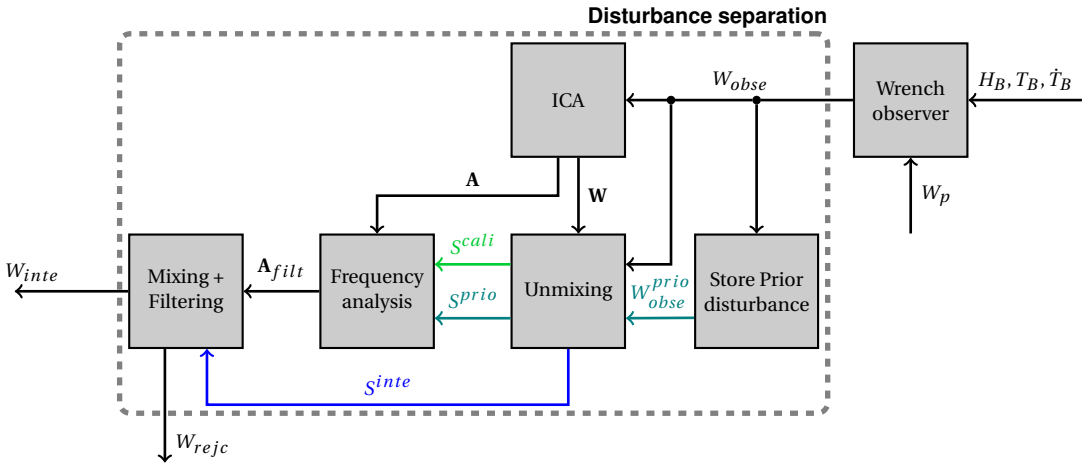

Figure 3.3: Disturbance separation block diagram detailed

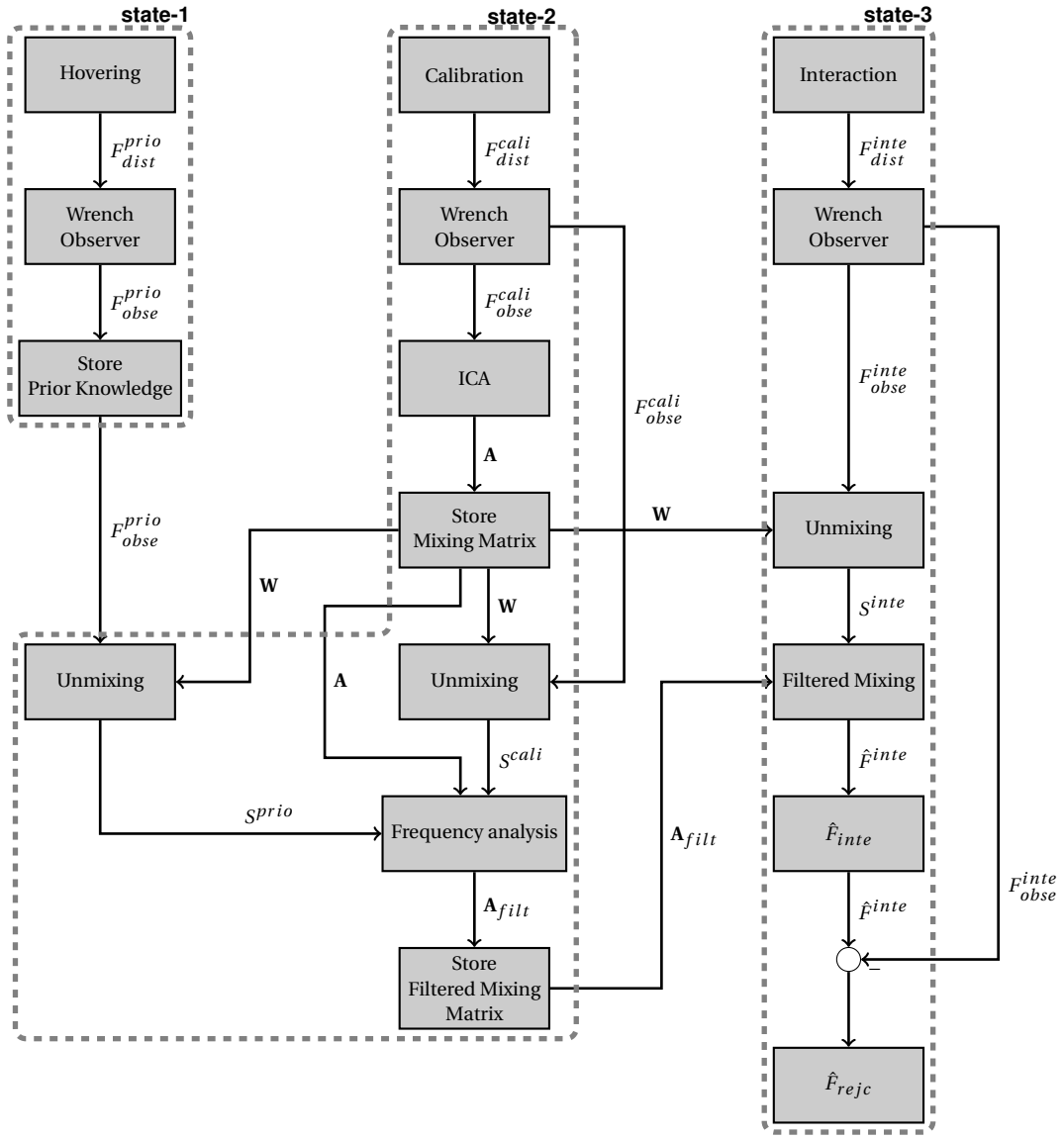

Figure 3.4: Data flow diagram

3.2.2 Separation configuration

In this thesis, the separation is performed offline on Python 2.7.12. For the experiment, there is some pre-processing that is performed in MATLAB because it has better support for parsing a rosbag compared to python module. Rosbag file is the format in which the experiment data is stored.

The independent component analysis is performed using available FastICA module which is part of scikit-learn module [15]. The provided Fast ICA module is using a fixed-point iteration algorithm and measures nongaussianity by maximizing negentropy. The negentropy is approximated using logcosh function.

The configuration of FastICA that is used in this thesis is shown in table 3.1.

Table 3.1: FastICA configuration

Parameter	Value
Algorithm	Parallel
Max iteration	200
N components	3
Tolerance	10^{-4}
Function	logcosh
Whiten	enabled

4 Simulation

In this chapter, detail of the conducted simulations will be presented. This chapter is separated into two sections. The first section will explain the simulation design while the second section will explain the result of the simulation.

4.1 Simulation design

The simulations are performed on 20-sim using a model of BetaX. The position control in BetaX is using impedance control; thus by setting position set point behind a wall, the UAV would push against the wall with force depending on distance difference between the wall, which limits UAV position, and position set point.

In the simulation, the UAV would interact with a model of a wall which already has the model of a contact impedance and friction model. Simulation of wind disturbance is added including an option to enable modeling error in the simulation.

As already mentioned in Chapter 1, the dimension of disturbance source is limited to the dimension of disturbance measurement. Thus, to satisfy the condition, the simulation is conditioned to meet the requirement by limiting the disturbance source. However, the limit of the method is also explored by increasing the dimension of the disturbance source beyond the dimension of disturbance measurement.

4.1.1 Simulation goals

The goals of performing the simulation are as follow:

1. To check the performance of the proposed separation method in simulated condition. The performance of the separation is measured by comparing the estimated interaction force from separation with the actual interaction force which is known in the simulation.

2. To check the limitation of the proposed separation method. Conditions where the separation failed to perform, will be checked, including increasing the dimension of the disturbance.

4.1.2 Environment setup

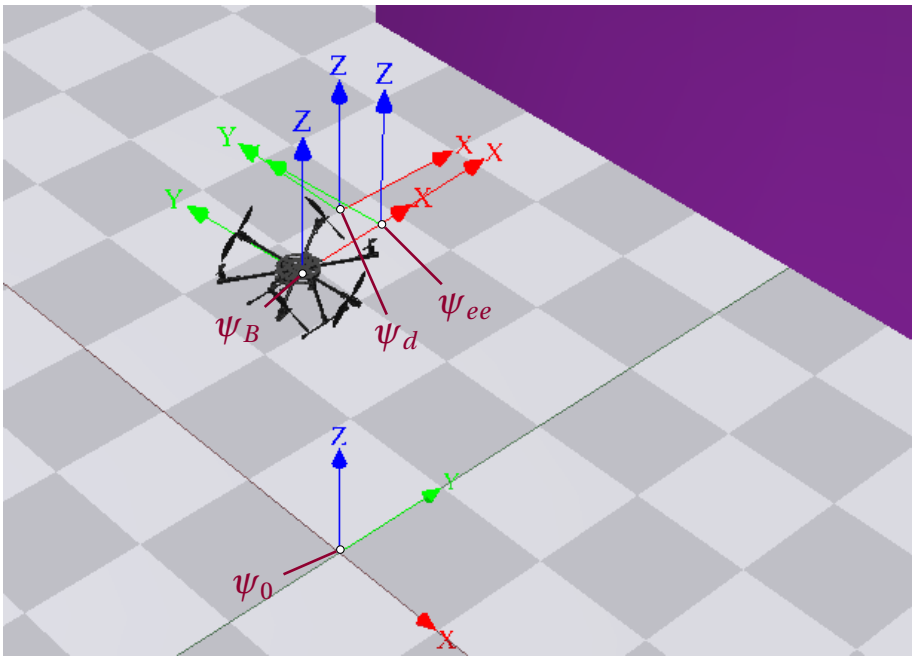

Figure 4.1: A screenshot for the simulated UAV in 20-sim including the reference for available frames

A screenshot of simulation animation in 20sim is shown in Figure 4.1. In the figure, the UAV is hovering above the world frame ψ_0. The end-effector frame ψ_{ee} of the UAV is controlled using impedance control with set point on frame ψ_d. The body frame of the UAV is indicated by ψ_B. The position error between ψ_d and ψ_{ee} is due to the wind disturbance that is blowing parallel to the X-axis of world frame ψ_0. The wall positioned in $y = 5\,\text{m}$ of world frame ψ_0. To match the sampling time which will be used in the experiment $T_s = 50\,\text{ms}$, the data from the simulation is down-sampled.

4.1.3 Simulation flight path

A desired flight path is prepared for the UAV. The path is prepared in such a way that it would only contribute two components of disturbance source. The path can be split into four parts:

Hover is when the UAV is hovering close to the wall that it is going to interact with. During this part, the separation process performs the hover state to gather disturbance sample prior to the interaction.

Sinus 1 is when the UAV is moving along the surface of the wall in X-axis world frame. The variable set point in X-axis is changed in the form of a sinusoidal wave. During this part, the separation process performs calibration state.

Sinus 2 is the same as the previous path with a bigger magnitude. During this part, the UAV already started performing the actual interaction.

Square is when the UAV is sliding along one axis of the wall with the position set point in the form of a square wave and bigger magnitude than the previous part.

Initially, the position of UAV body frame ψ_B is at ψ_0. The desired path of the UAV is shown in Figure 4.2 and Figure 4.3.

From the per-axis view, the previously mentioned four parts of the desired flight path can be seen. From the figure, it can be seen that the UAV is sliding along X-axis while setting a constant value in both Y and Z-axis. In the 3D plot of the desired flight path, the path follows the 'Viridis' colormaps which started from dark purple and ended with light yellow.

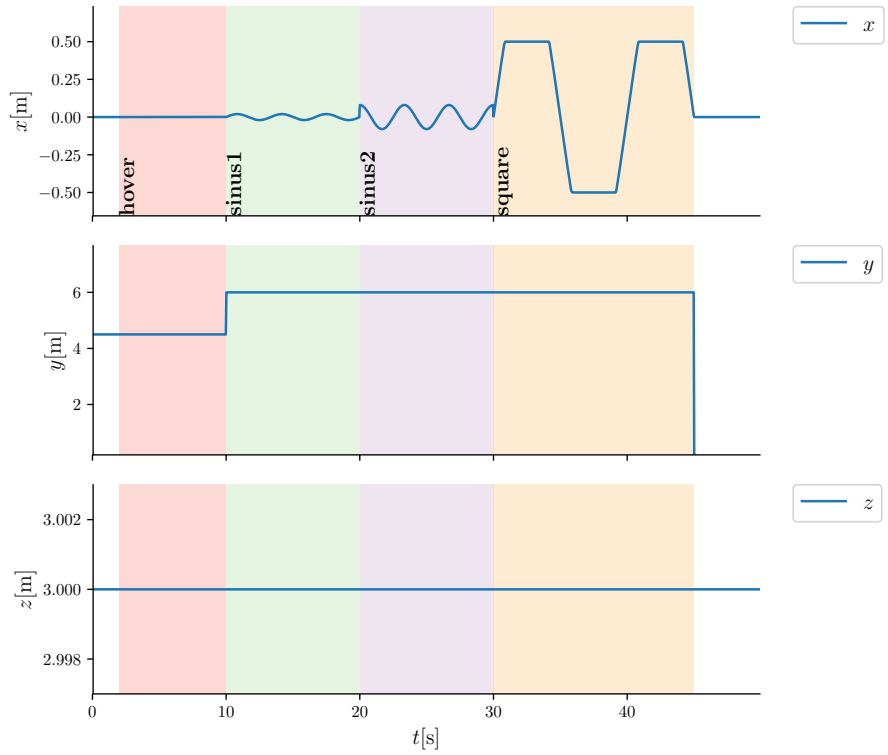

Figure 4.2: Desired flight path in per-axis, each dashed area represent different part of flight path.

From the 3D figure, it can be observed that the desired position of the UAV during interaction is located behind the wall. Since the UAV uses impedance control, the difference between actual position and desired position will generate control force. The desired path in the Y-axis is linear to the normal force from the wall to the UAV, while the desired path in the X-axis is linear to the wall friction force.

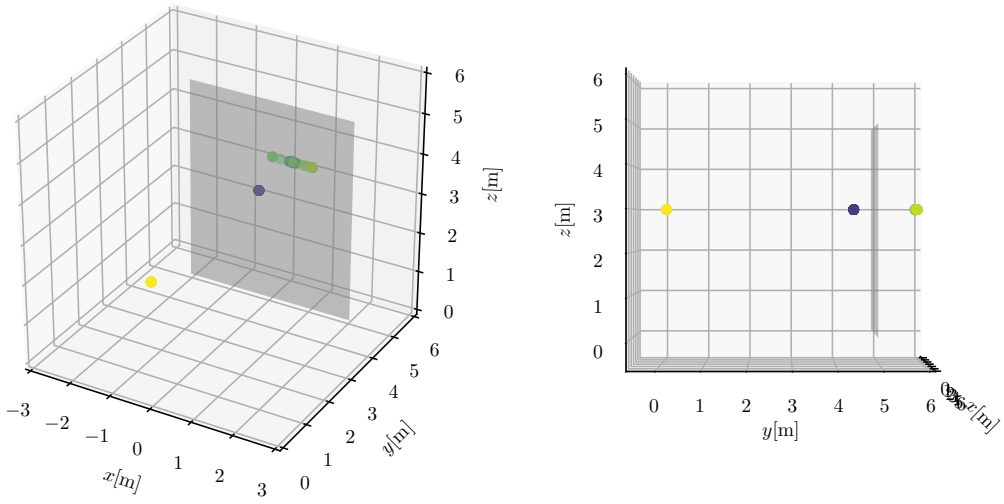

Figure 4.3: The desired flight path in 3D. Perspective view (left) and side view (right). The desired path started from dark purple and ended in light yellow. Transparent gray surface represents the wall.

4.1.4 Scenarios

Several scenarios are prepared to add disturbances to the UAV. Below are the prepared scenarios:

No disturbance is a scenario where there are no additional disturbances.

Wind disturbance is the scenarios where wind disturbance is added. By default, the wind is blowing along the X-axis of the world frame ψ_0. This scenario is varied by rotating the wind about the Z-axis of ψ_0.

Modeling Error is the scenario where an error in the model of the UAV is simulated. It is performed by intentionally making the assumption that is made during the design of UAV control incorrect. The assumption that is made incorrect is the mixing-matrix[1] M which relates angular velocity of each UAV's propeller to thrust acting on UAV's body. The specific part of M matrix that is changed is the tilt angle of the UAV's propeller to give significant effect.

4.1.5 Source of disturbances

During the simulation, there are three components of disturbances: interaction, aerodynamic, and modeling error. In this part of the report, each disturbances model and the assumption in the simulation will be explained.

Interactions

Two disturbances are generated as consequences of the interaction between UAV end-effector with the wall surface. Those disturbances are contact impedance and friction. The interaction disturbance expressed in ψ_0 is

$$F_{inte}(t) = \begin{bmatrix} F_{x,fric} \\ F_{y,cont} \\ 0 \end{bmatrix} \tag{4.1}$$

[1] Not to be confused with the mixing matrix of ICA.

The force from contact impedance is modeled after simple linear spring and viscous damper model of Kelvin-Voight

$$F_{cont}(t) = \begin{cases} Kx(t) + B\dot{x}(t), & x \geq 0 \\ 0 & x < 0 \end{cases}. \tag{4.2}$$

with $x(t)$ as the penetration depth of UAV end-effector into wall surface and $\dot{x}(t)$ as the velocity of the penetration. The value of the stiffness coefficient is $K = 2260\,\mathrm{N/m}$ while the value of the damping coefficient is $B = 123\,\mathrm{Ns/m}$.

A viscous friction model is used to describe opposing force during movement along the surface of the wall. The equation of the viscous friction is

$$F_{fric}(t) = \mu_s \cdot \dot{x}(t), \tag{4.3}$$

with viscous friction coefficient defined as $\mu_s = 0.1\,\mathrm{Ns/m}$.

Wind Disturbances

In the simulation, the wind is modeled as a combination of constant value, sinusoidal signal, and Gaussian noise which then rotated based on the scenario used. The aerodynamic disturbance is described as

$$F_{aero}(t) = R \cdot \begin{bmatrix} A + B\sin\left(2\pi f t\right) + C \cdot \mathrm{gauss}(t) \\ 0 \\ 0 \end{bmatrix} \tag{4.4}$$

with R as rotation matrix, A as a constant value of 2 N, B as a magnitude of sinus component of 0.1 N, f as a frequency of a sinusoid signal of 3 Hz and C as a magnitude of Gaussian noise of 0.1 N. The rotation matrix is rotated along the Z-axis of ψ_0.

$$R = \begin{bmatrix} \cos(\theta) & -\sin(\theta) & 0 \\ -\sin(\theta) & \cos(\theta) & 0 \\ 0 & 0 & 1 \end{bmatrix} \tag{4.5}$$

Modeling error

In the UAV model, the relation between the angular velocity of the propellers and the wrench vector value which they applied to the UAV body is explained as follow

$$W_{\text{props}}^{\top} = \begin{pmatrix} \tau_x \\ \tau_y \\ \tau_z \\ F_x \\ F_y \\ F_z \end{pmatrix} = \mathbf{M}\left(p_{\text{props}}, \alpha\right) \cdot \begin{pmatrix} |\omega_1|\omega_1 \\ |\omega_2|\omega_2 \\ |\omega_3|\omega_3 \\ |\omega_4|\omega_4 \\ |\omega_5|\omega_5 \\ |\omega_6|\omega_6 \end{pmatrix}. \tag{4.6}$$

The propeller wrench W_{props} is the result of multiplication between a constant propeller mixing matrix[2] M—which is a 6 by 6 matrix of the 6 propellers which is the function of propeller position p_{prop} and the tilt of the propeller along its arm α—and "sign-squared" of each propeller angular velocity ω_i. To generate a desired angular velocity from a desired W_{props} the inverse of mixing matrix is used

$$|\omega_{\text{des}}|\,\omega_{\text{des}} = \mathbf{M}^{-1} \cdot W_{\text{props}}^{\top}. \tag{4.7}$$

To produce a modeling error, an inverse mixing matrix with an incorrect parameter is prepared. To signify the effect, the tilt angle of the propeller α is chosen to be the one that is going to be changed.

[2] Not to be confused with ICA mixing matrix

The actual tilt of the propeller is 45° angle along the arm where it is mounted at, while the modeling error tilt angle is set at 47°

4.2 Simulation results

In this section, the result of the simulation will be presented. This section will be delivered as follow:

First, the statistical properties of observed disturbance of each scenario will be compared against actual interaction force.

Second, the correlation of each independent components for each scenario will be shown.

Third, an example of the separation process will be shown.

Fourth, the statistical property of the separation of each scenario will be shown.

4.2.1 Observed disturbance of simulation

The effect of different disturbances toward the observed disturbance will be explained in this subsection. The effect will be grouped into two parts. The first one is to compare different wind orientation to the observed disturbance. The second one is to check the effect of the modeling error.

Effect of wind direction to observed disturbance in simulation

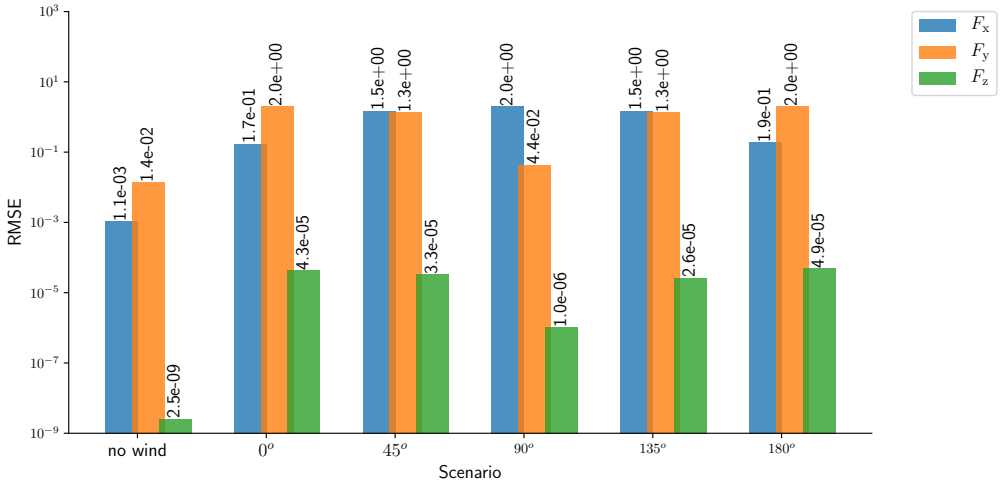

(a) RMSE per-axis

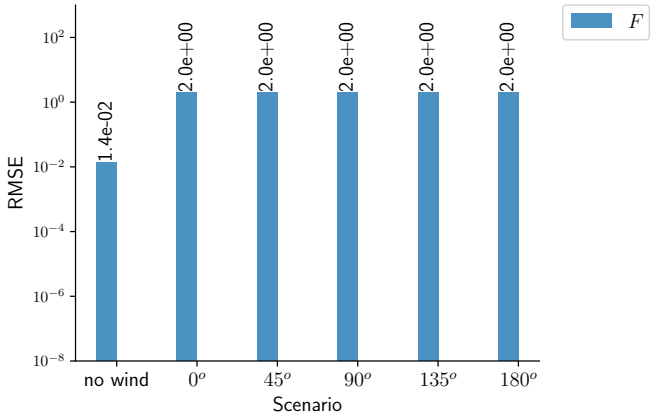

(b) Total RMSE

Figure 4.4: RMSE of wrench observer $\hat{F}_{dist}$ against actual interaction F_{inte} with scenarios of different wind orientation

In Figure 4.4, the Root Mean Square Error (RMSE) between F_{inte} and F_{obse} with scenarios of different wind orientation are shown. From the per-axis plot, it can be seen that the error in X-axis and Y-axis changes according to the direction of the wind. It can be seen that the disturbance in X-axis is the highest when the orientation angle of the wind is at 90° since the wind is aligned with the X-axis. However, the sum of the of the RMSE is the same since the total magnitude of the wind is the same.

Effect of modeling error to observed disturbance in simulation

In Figure 4.5, the RMSE between F_{inte} and F_{obse} with modeling error scenarios are shown. In the RMSE per-axis, it is apparent that the error of each axis is increased when the modeling error is activated, and indeed, when the wind disturbance is added in Y-axis, the disturbance in Y-axis increased. The total RMSE increased when the modeling error is activated.

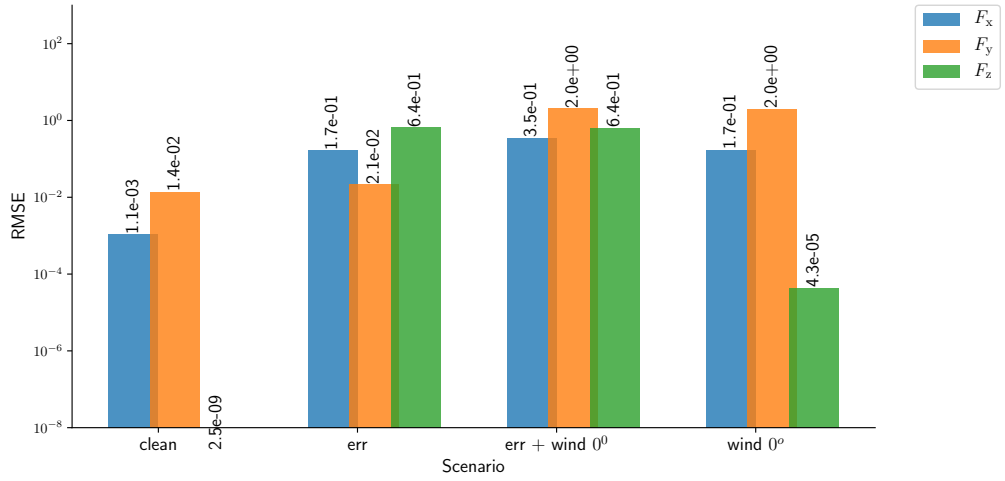

(a) RMSE per-axis

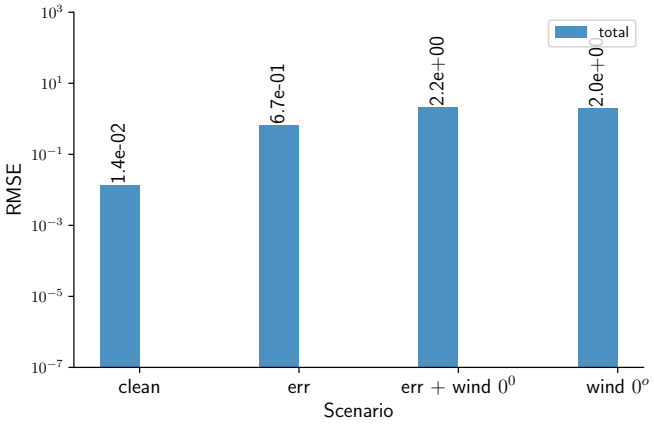

(b) Total RMSE

Figure 4.5: RMSE of wrench observer $\hat{F}_{dist}$ against actual interaction F_{inte} with scenarios of modeling error

4.2.2 Example of separation process

In this part of the report, an example of a separation process is presented. The scenario which will be presented is the one where the wind is oriented 45°. In this subsection data from the simulation which includes position, disturbances, including data from the separation process will be shown.

Actual position

As explained in the simulation setup subsection 4.1.3, the UAV will follow through a pre-planned path. The actual path of the UAV is shown in Figure 4.6, 4.7, and 4.8. From the per-axis plot of the actual position, it can be seen that the position of the UAV on Y-axis is limited at 5 m due to the position of the wall.

The position of the wall is well shown in the 3D figure of the UAV path. In the 3D figure, the UAV path started from the dark purple color and ended with the light yellow color. UAV path during the interaction could better be seen in the zoomed version of the 3D figure where it is quite clear that the UAV is only moving along the X-axis during the interaction.

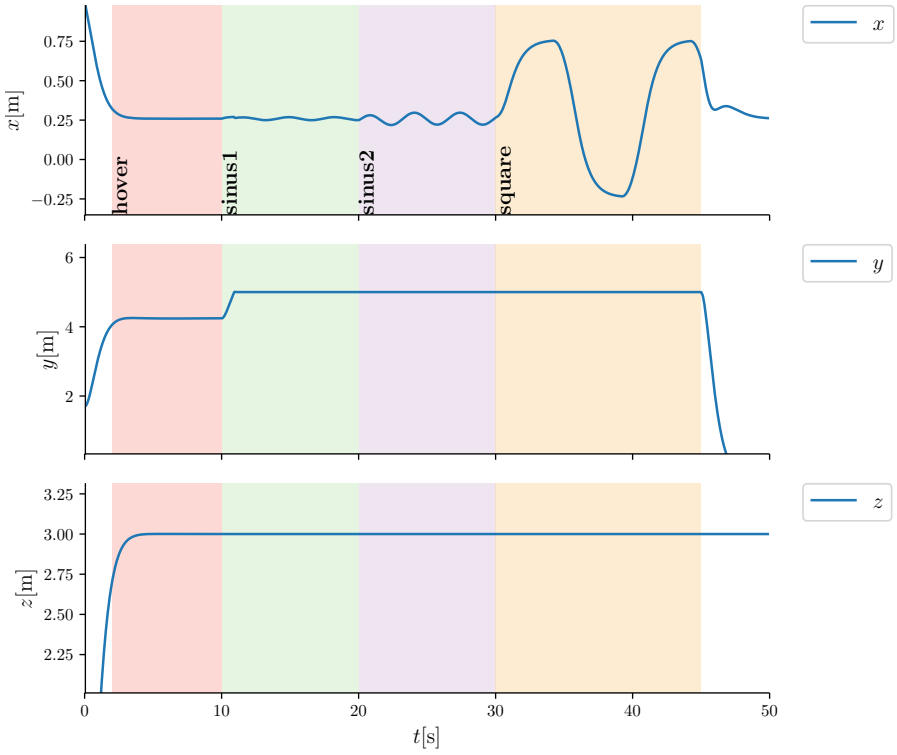

Figure 4.6: Actual path of UAV per-axis

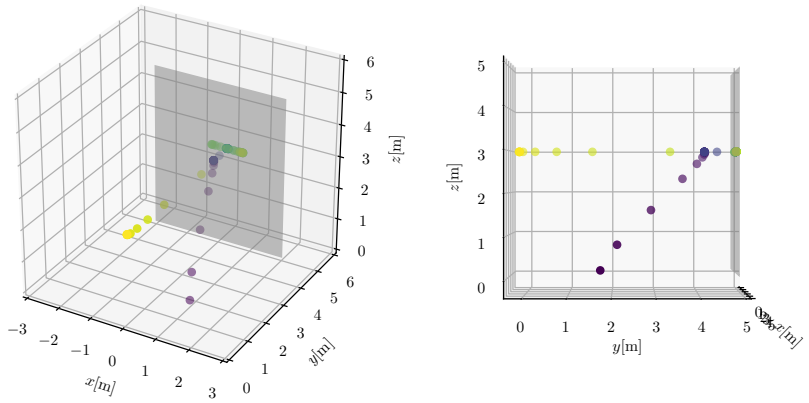

Figure 4.7: Actual path of the UAV in 3D, perspective view (left) and side view (right)

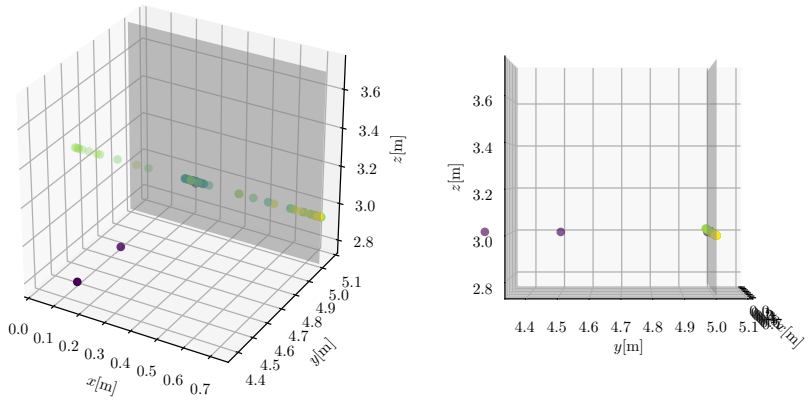

Figure 4.8: Actual path of the UAV in 3D, zoomed, perspective view (left) and side view (right)

Disturbances and its components

Figure 4.9 shows the disturbance force of the UAV in the end effector frame ψ_{ee}. It shows that the total disturbance consists of aerodynamic disturbance and the interaction disturbance. Even though wind the direction of the wind disturbance during the interaction is static. Due to the movement of the UAV, the wind disturbance in the end effector frame changes a bit [3].

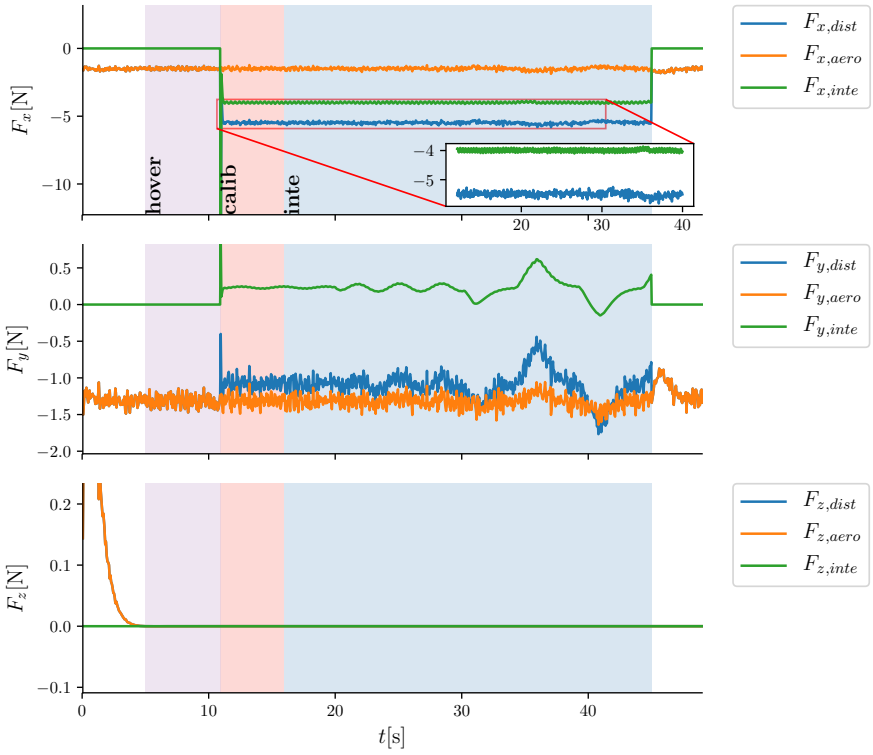

Figure 4.9: Disturbance and its components

[3] Even though it is a fully-actuated UAV; there are still small changes in its orientation.

Disturbances observer

Figure 4.10 shows the force component of the output of the wrench observer. In the figure, the output of the wrench observer is compared against the actual disturbance. From comparing both forces, it can be seen that the observed disturbance is a low-passed version of the actual disturbance which can be seen from the fewer high-frequency noise and slight lag from the actual one.

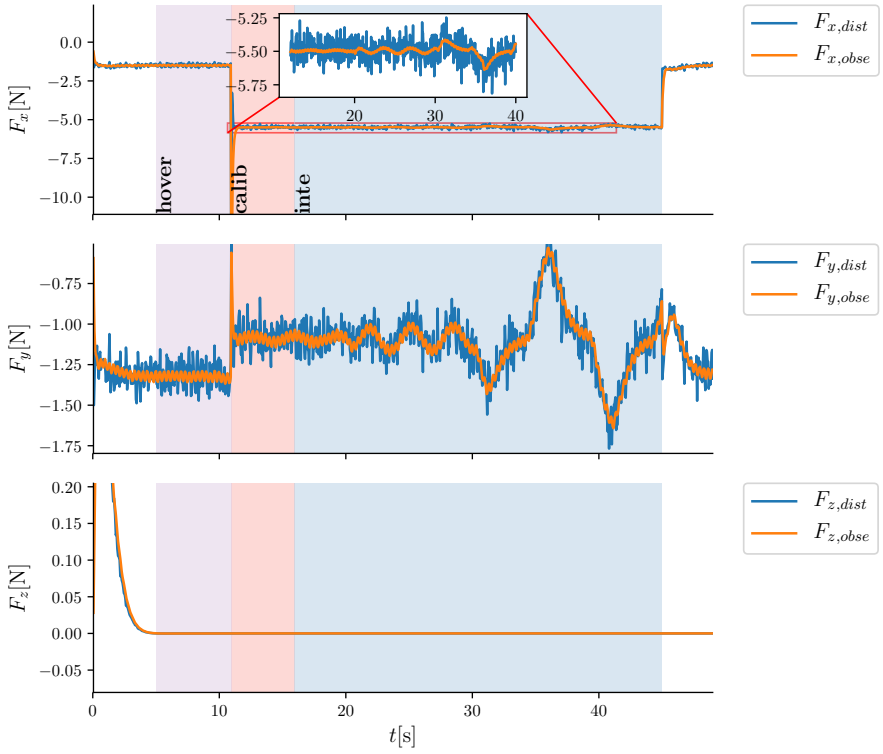

Figure 4.10: Comparison between wrench observer output and actual disturbance

As stated during the introduction, the goal of this thesis is to be able to separate interaction from the output of the wrench observer. The comparison between wrench observer output and the actual interaction force can be seen in Figure 4.11. By comparing both signals, it is apparent that the observed disturbance is equal to interaction force with mixed with aerodynamic disturbance. The distinctive effects of the addition of wind disturbance are the high-frequency sinusoid signal and the constant value of around 1.3 N in the X and Y-axis of observed disturbance. The error plot between observed disturbance and actual interaction force is shown in Figure 4.12. The figure shows that the error is not only contributed to aerodynamic disturbance, but also from the lag between observed disturbance and actual disturbance.

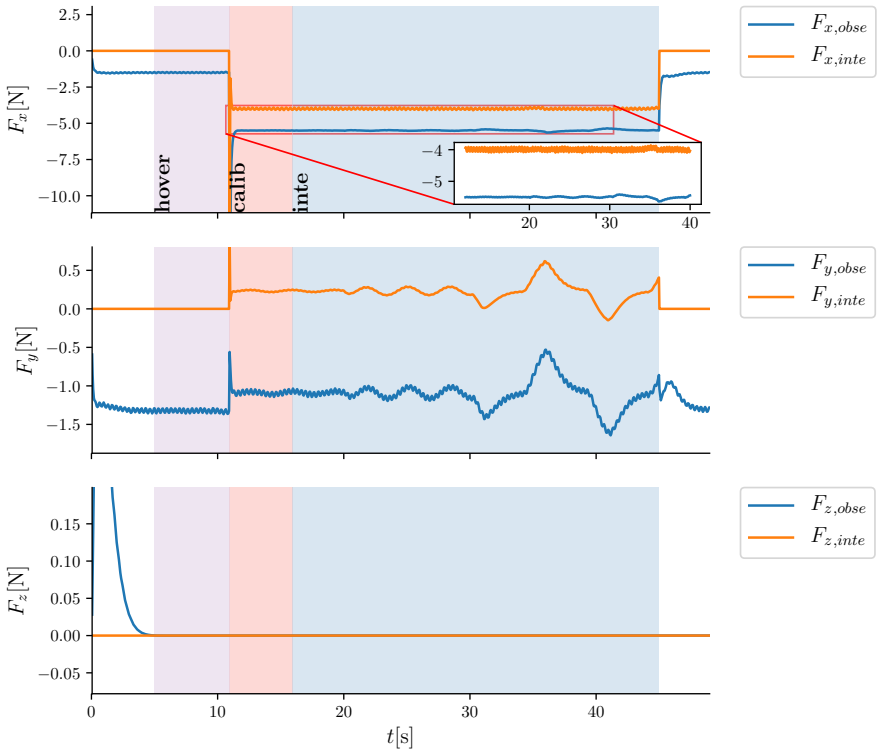

Figure 4.11: Comparison between observed disturbance and interaction force

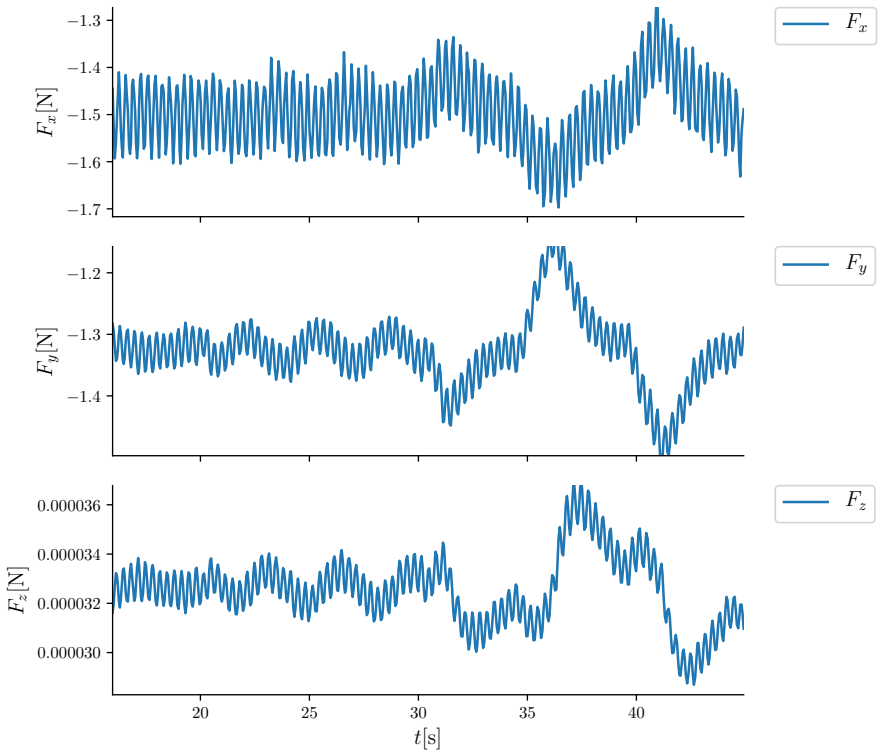

Figure 4.12: Error plot between observed disturbance and actual interaction force

Unmix observed disturbance using ICA

The process of separation is started by acquiring the unmixing matrix **W**. This is done by fitting observed disturbance during calibration[4] phase to ICA. The estimated unmixing matrix is

$$\mathbf{W} = \begin{bmatrix} -8.26 \cdot 10^{-2} & 7.06 \cdot 10^{-2} & 5.11 \cdot 10^{-2} \\ -2.20 \cdot 10^{-1} & -4.24 \cdot 10^{0} & -6.78 \cdot 10^{-1} \\ 7.91 \cdot -10^{3} & 7.52 \cdot 10^{-2} & -8.91 \cdot 10^{0} \end{bmatrix}. \tag{4.8}$$

Using the unmixing matrix, the observed disturbance is unmixed into independent component (IC). Figure 4.13 shows the IC of observed disturbance. From the figure, it is recognizable that S_0 and S_1 are contributed by interaction disturbance while S_2 is from wind disturbance.

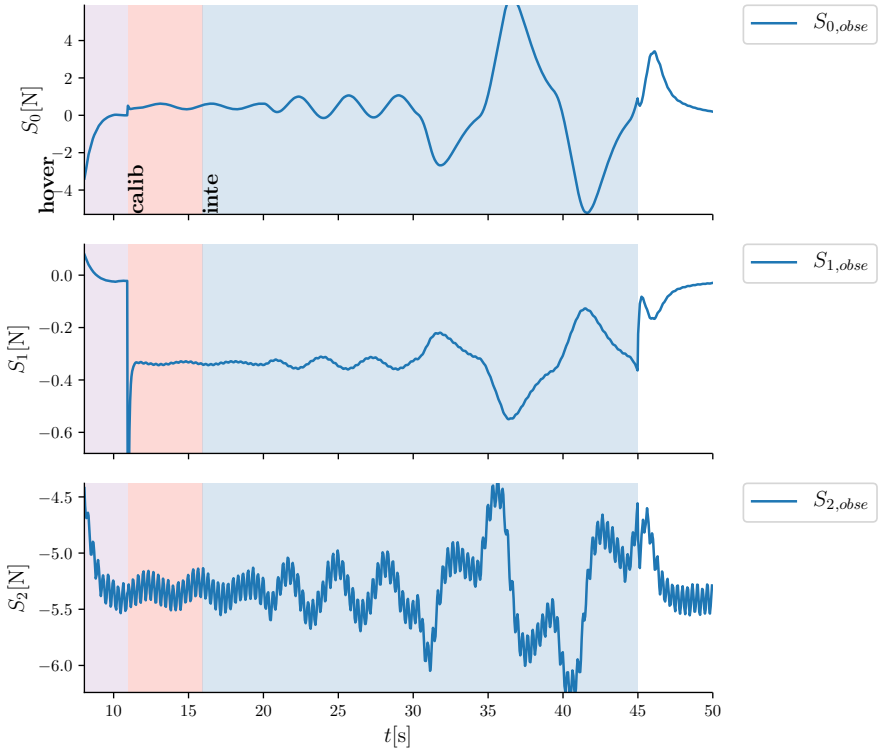

Figure 4.13: Independent component (IC) of wrench observer

[4]The observed that is fitted to ICA is shown in Figure 4.10. The fitted signal is sampled from observed disturbance with timespan marked 'calib' label.

4.2.3 Determine similar IC between hovering and calibration state

The next step is to determine which component that is similar between hovering and calibration state. As already mentioned in chapter 3, the first step is to transform the signal to the frequency domain using FFT with the result can be seen in Figure 4.14. Similarity coefficient, which is also defined in chapter 3, is then determined for each IC with result can be seen in table 4.1.

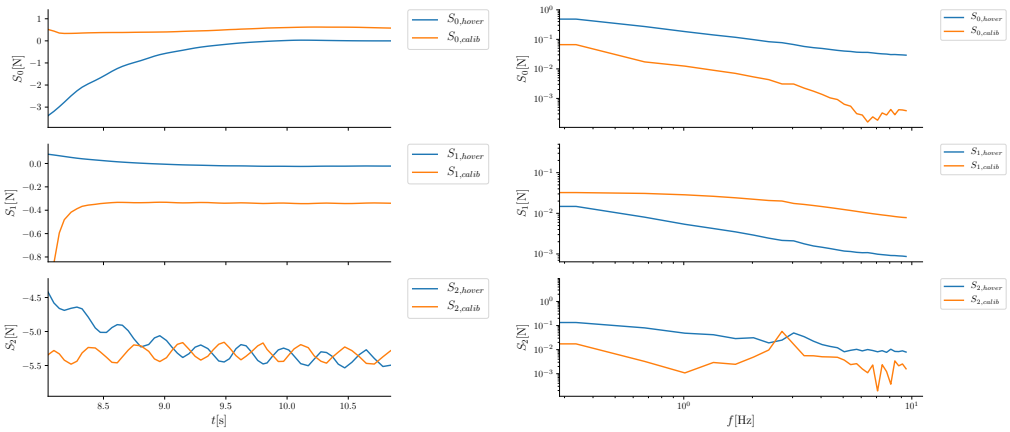

(a) Time domain **(b)** Frequency domain

Figure 4.14: Sampled Independent Components of hover and calibration state.

Table 4.1: Similarity coefficient for each IC

IC	RMS
S_0	$1.14 \cdot 10^{-1}$
S_1	$6.95 \cdot 10^{-2}$
S_2	$4.02 \cdot 10^{-2}$

By looking at the RMS value, it is determined that the IC that is similar between hovering and calibration state is S_2. Using this knowledge and the inverse of the unmixing matrix, a new mixing matrix with the column which correlates to wind disturbance is generated. The filtered-mixing matrix is determined as

$$\mathbf{A}_{\text{filt}} = \begin{bmatrix} 4.72 \cdot 10^{-1} & 1.35 \cdot 10^{+1} & 0 \\ 4.78 \cdot 10^{-2} & -6.51 \cdot 10^{-1} & 0 \\ 2.11 \cdot 10^{-6} & 8.22 \cdot 10^{-6} & 0 \end{bmatrix}. \tag{4.9}$$

Re-mix the independent component

Using the newly generated filtered-mixing matrix, the IC of observed disturbance is transformed back into its original space and become the estimated interaction force. The comparison between estimated interaction force and the actual interaction force is shown in Figure 4.15 with the error plot is shown in Figure 4.16.

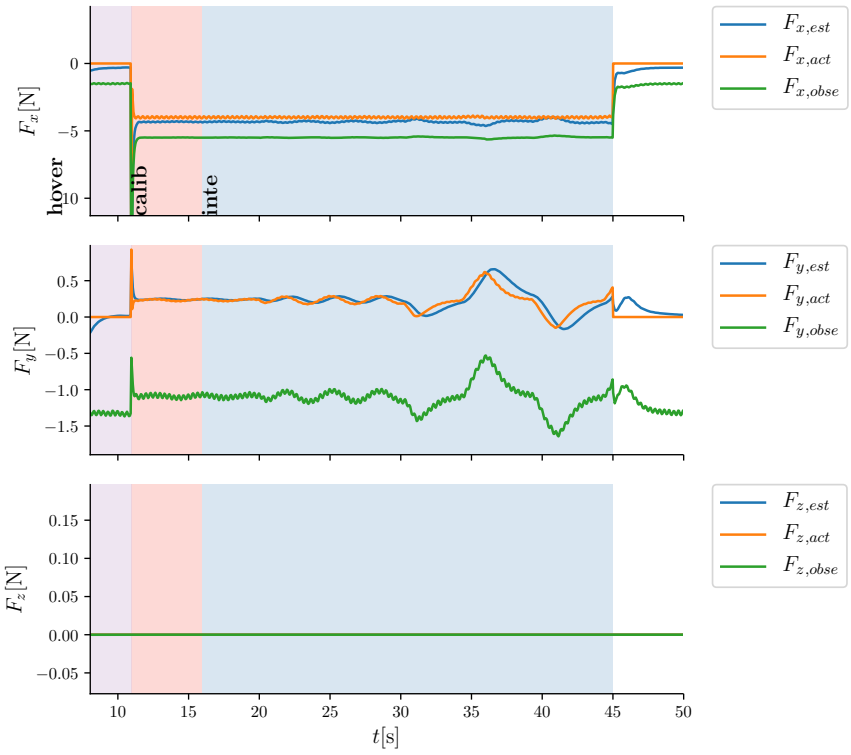

Figure 4.15: Estimated interaction force

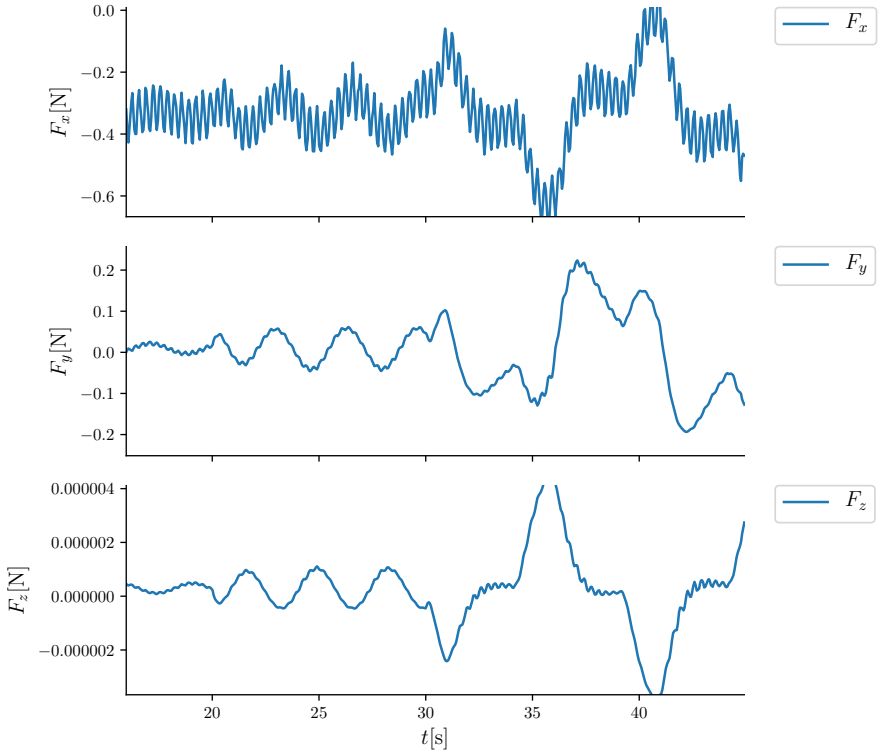

Figure 4.16: Estimated interaction force error

4.2.4 Independent component similarity coefficient between hovering and calibration state

Figure 4.17 shows the similarity coefficient of each IC for each scenario. From the bar plot it can be seen that in some cases, the difference between the lowest coefficient to the next lowest one is considerably small.

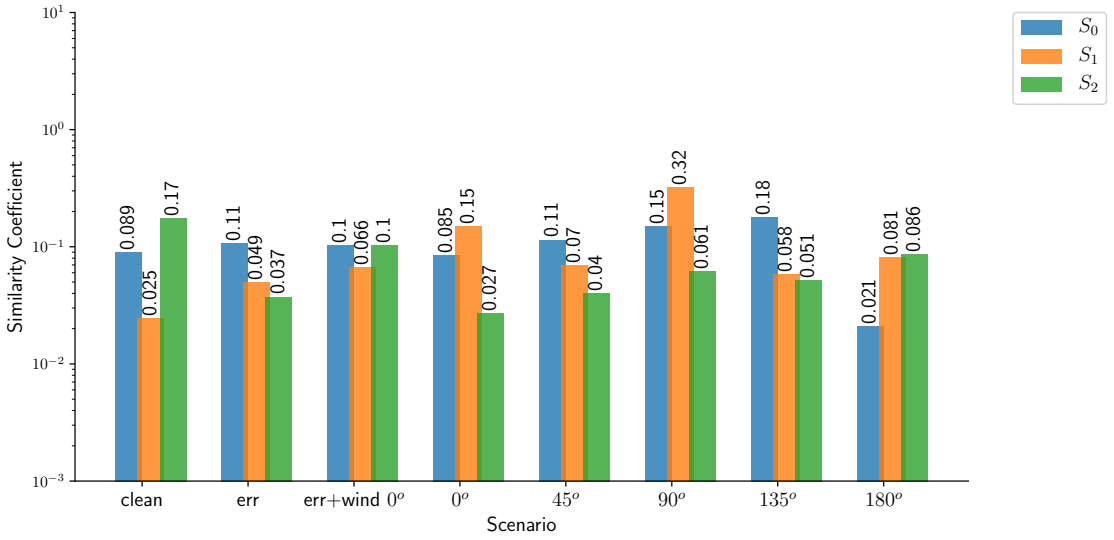

Figure 4.17: RMS of each IC between hovering and calibration state

4.2.5 Estimated interaction of simulation

In this subsection, the effect of different disturbances toward the estimated interaction from separation will be explained in this subsection. The effect will be grouped into two parts. The first one is to compare different wind orientation to the observed disturbance, and the second one is to check the effect of the modeling error.

Effect of wind orientation to disturbance separation in simulation

In Figure 4.5, the effect of wind direction to the disturbance separation can be seen. The bar plot shows the RMSE between the estimated interaction force $\hat{F}_{inte}$—which is the result of the separation—against the actual interaction force F_{inte}. The per-axis figure shows that the separation is optimum when the wind is perpendicular with the vector of the interaction. It is also confirmed by observing the total RMSE.

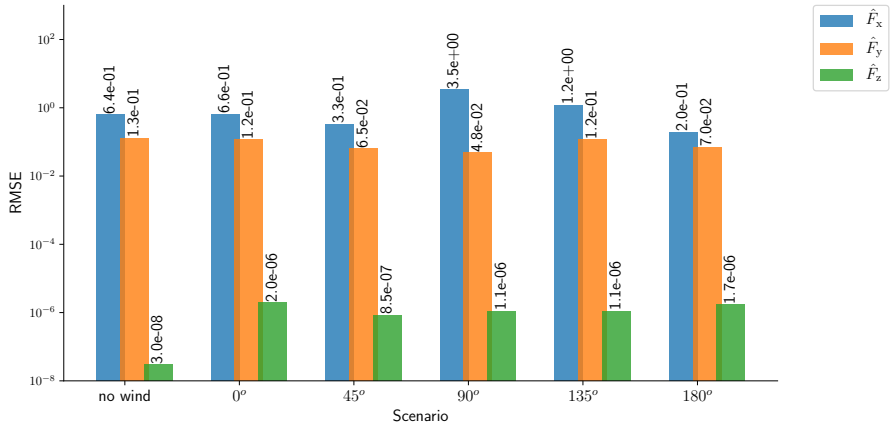

(a) RMSE per axis

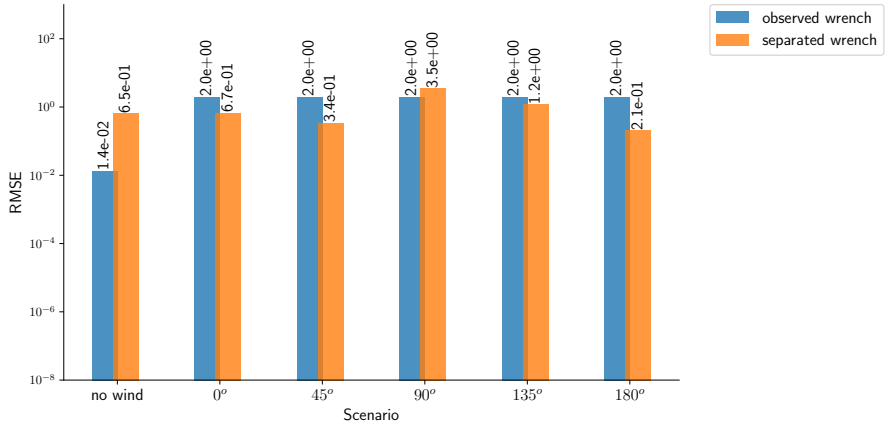

(b) Total RMSE compared with observer data

Figure 4.18: RMSE of estimated interaction force

From the bar plot of the RMSE, there are two scenarios where the RMSE of the separation is worse than the RMSE of the initially observed disturbance. The first one is the scenario with no disturbance, and the other one is where the wind orientation angle is 90°.

To be able to analyze those scenarios, the independent component (IC) of both scenarios are presented. Figure 4.19 shows the IC of no-disturbance scenario. It can be observed that the IC is not independent. This results in a failed separation.

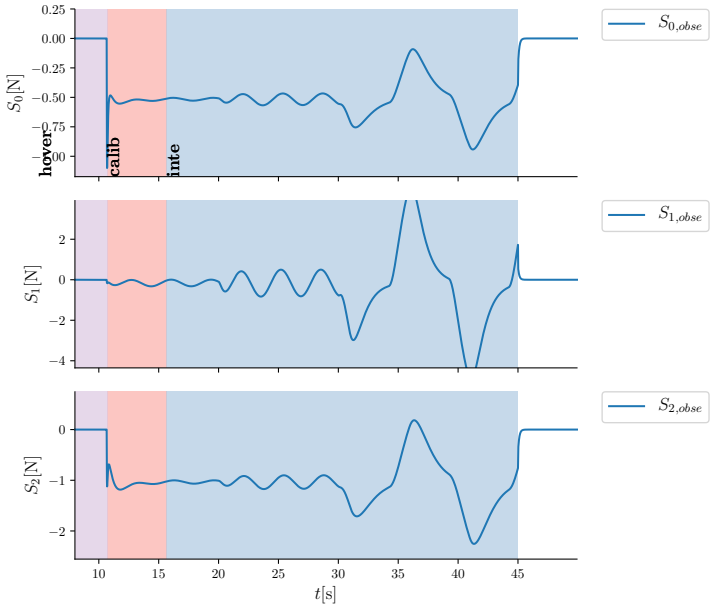

(a) Complete data

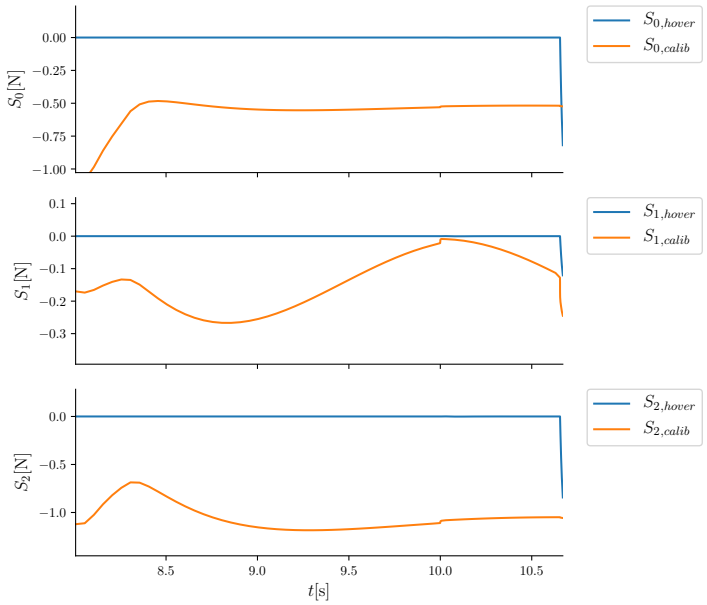

(b) Comparison between hover and calibration state

Figure 4.19: Independent component (IC) of no-disturbance scenario

Figure 4.20 show the IC of 90° wind orientation. It also shows that the IC is not independent which caused a poor separation performance.

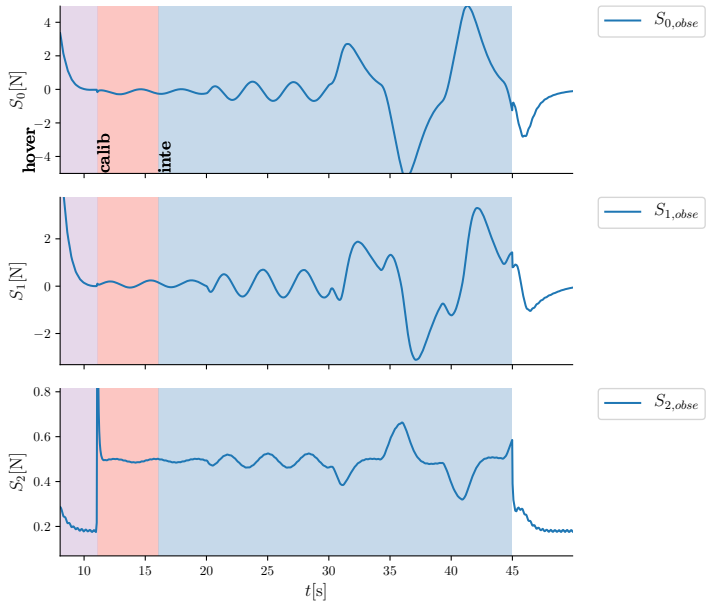

(a) Complete data

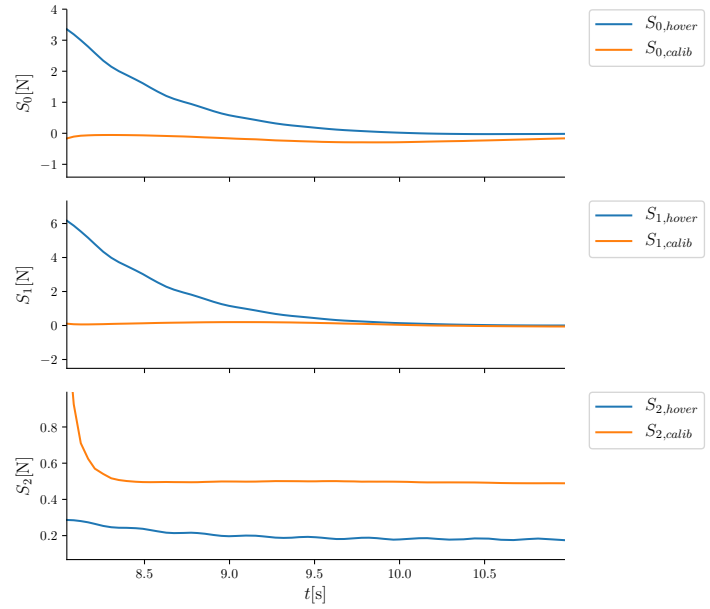

(b) Comparison between hover and calibration state

Figure 4.20: Independent component (IC) of 90° scenario

Effect of modeling error to disturbance separation in simulation

Figure 4.21 show the RMSE of different scenarios which involves modeling error. From the total RMSE bar plot, it is apparent that the performance of separation with modeling error scenario gave bigger RMSE compared to the initially observed disturbance. Which means the separation method failed to estimate the interaction force.

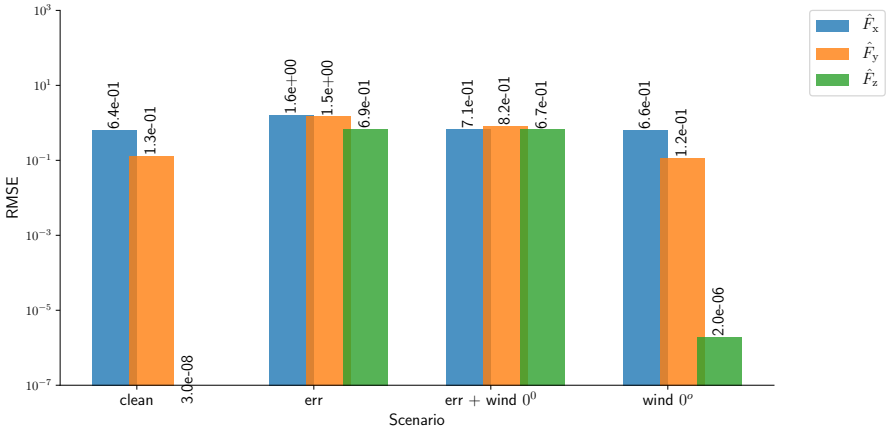

(a) RMSE per axis

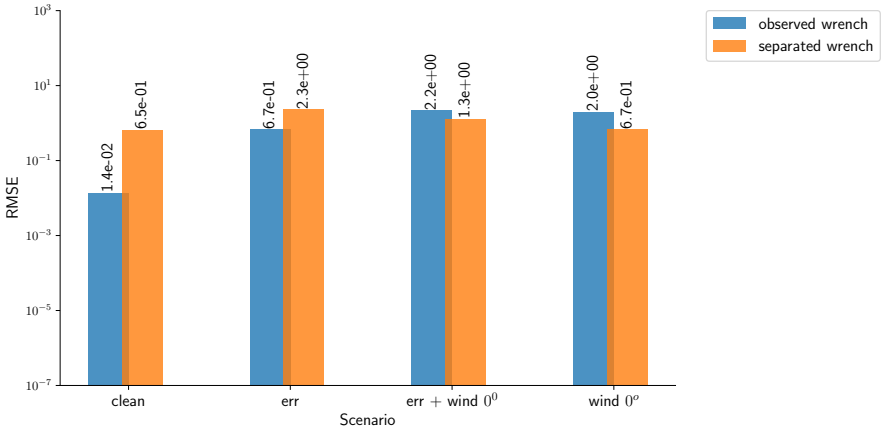

(b) Total RMSE compared with observer data

Figure 4.21: RMSE of estimated interaction force

Figure 4.22 shows the IC of the modeling error scenario. From the comparison plot, it can be seen that there is no similarity between each IC which indicate ICA could not separate modeling error into a single IC.

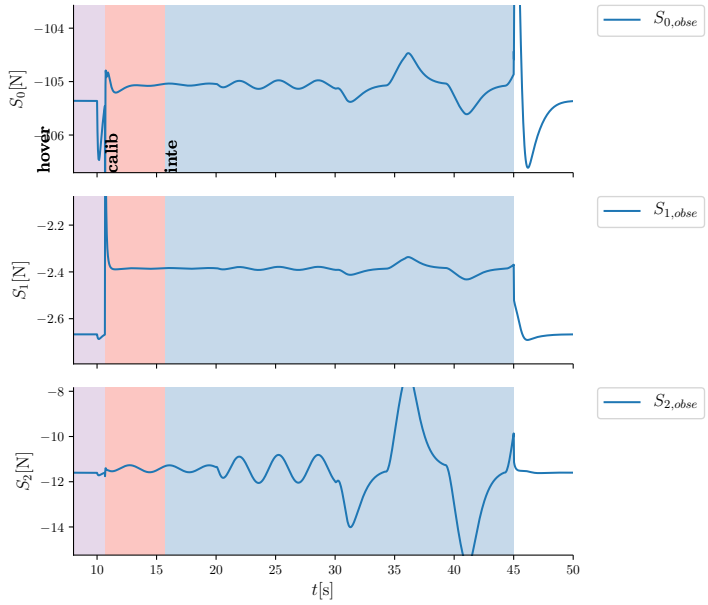

(a) Complete data

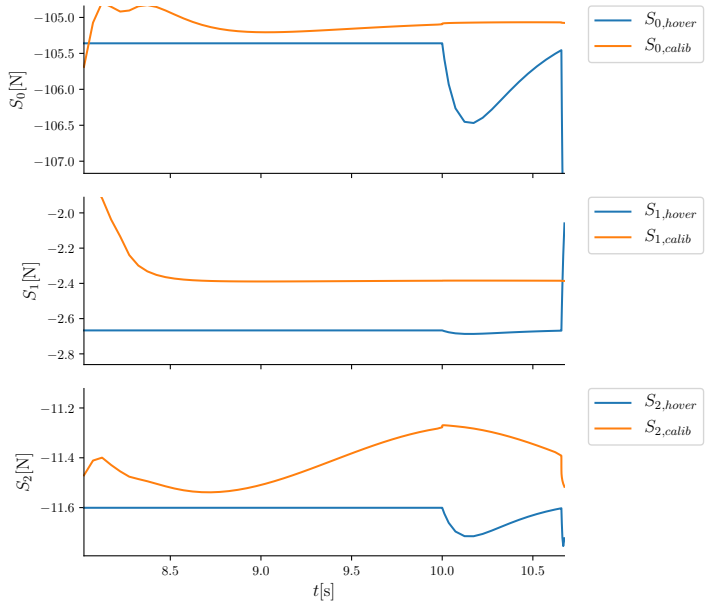

(b) Comparison between hover and calibration state

Figure 4.22: Independent component (IC) modeling error scenario

5 Experiments

In this chapter, detail of the conducted experiments will be presented. This chapter is separated into two sections. The first section will explain the design of the experiments. The second section will explain the result of the experiments.

5.1 Experiment designs

The experiments are performed using BetaX, a fully-actuated hexarotor, in SmartXP lab with motion capture camera facility. A sensor platform with a flat surface attached to a torque sensor is provided as ground truth of the interaction force.

5.1.1 Experiment Goals

The goals of the experiments are as follow:

1. To check the performance of the proposed method in real-world condition. The performance of the separation is measured by comparing the estimated force from separation with the actual force data which is taken from the reading of a torque sensor that is attached with a plate where the UAV is interacting with.
2. To evaluate the real-world implementation of the separation.

5.1.2 Experiment environment setup

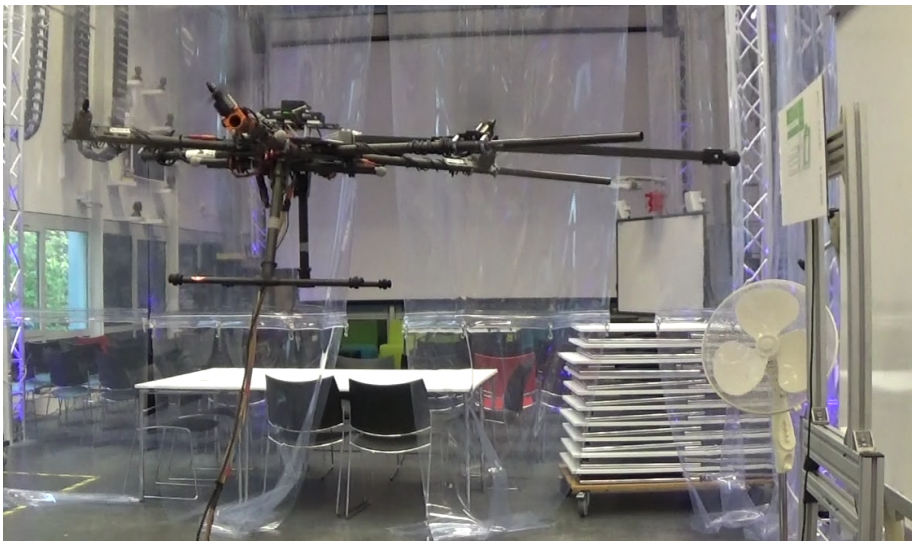

Figure 5.1: A picture of BetaX during experiment at SmartXp lab with standing fan (background) and sensor platform (right)

The experiment is performed in SmartXp laboratory of the University of Twente. The laboratory provides a dedicated area for UAV experiments which is protected by a transparent curtain to have a safe operation, see Figure 5.1. The area is also is also equipped with multiple OptiTrack motion capture camera. By having the OptiTrack camera, the dynamic of the UAV— including its position, velocity, and acceleration of both angular and translational—is known.

To get a reference for ground-truth a torque sensor is mounted on top of a portable structure. The height of the sensor is around 1.5 m to minimize ground-effect. A plate, made of acrylic, is mounted on top of the sensor as a platform for the UAV to interact with. The design of the sensor and its structure can be seen in Figure 5.2.

(a) Portable sensor platform

(b) Interaction plate which is mounted on top of the torque sensor

Figure 5.2: Torque sensor platform

5.1.3 Experiment flight path

The flight path for the experiment is controlled manually using an in input from a ROS in a computer. The path can be split into three parts:

Hover is when the UAV is hovering close to the wall that it is going to interact with. During this part, the separation process performs the hover state to gather disturbance sample prior to the interaction.

Pushing is when the UAV is pushing against the sensor. This state could be set up as a calibration state or actual interaction

Sliding is when the UAV is sliding along the surface of the sensor. This state could be set up as a calibration state or actual interaction

An example of the flight path can be seen in Figure 5.3 and Figure 5.4. The example that is shown in this report is from exp4. As mentioned in the previous section, this experiment provided an additional movement in Y-axis and Z-axis.

Unlike the simulation, where the desired flight path is identical for each scenario, the flight path in the experiment is manually controlled through a graphical user interface (GUI) for robot operating system (ROS).

From the 2D figure, it can be observed that the changes in the desired position of the UAV is not as fluent as the one from the simulation. The height of the sensor position can also be

observed from the UAV path, which is 1.5 m. From the 3D figure, it can also be seen that during the interaction, the UAV is only pushing against the sensor plate.

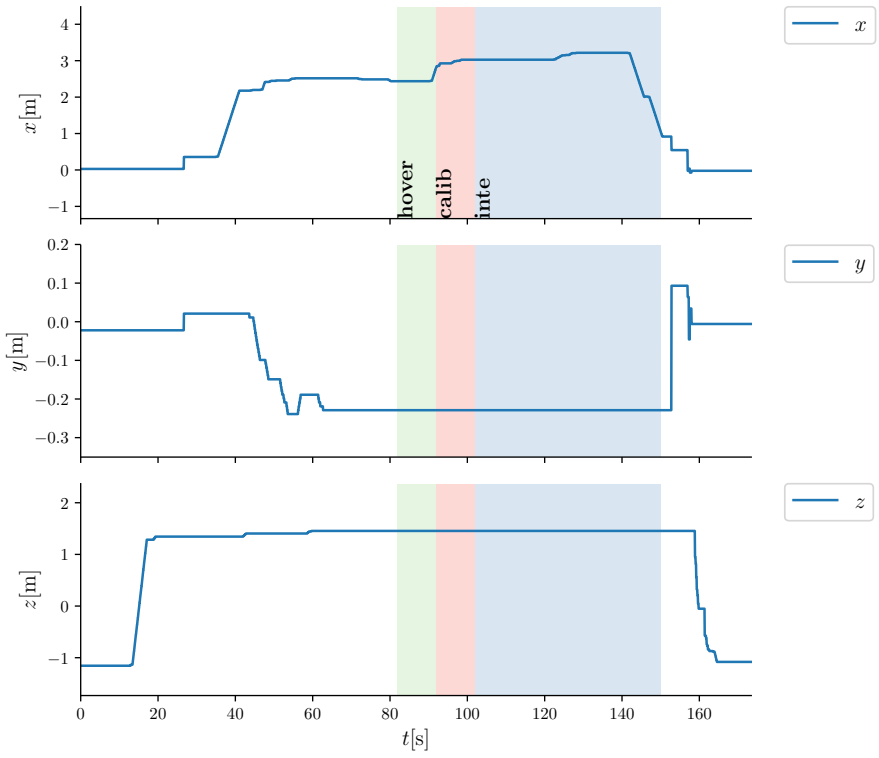

Figure 5.3: The desired flight path in per-axis. The dashed area color represent the assigned separation state.

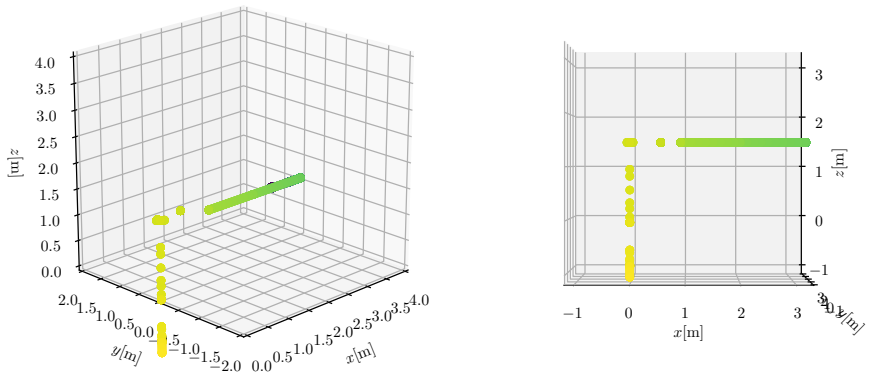

Figure 5.4: The desired flight path in 3D. Perspective view (left) and side view (right). The desired path started from dark purple and ended in light yellow.

5.1.4 Scenarios

For the experiments, five scenarios are prepared. The list of the scenarios consists of

exp1 In this scenario, the UAV interact with the sensor by pushing against it. The fan is not activated and without the screen positioned behind the sensor.

exp2 In this scenario, the UAV interact with the sensor by pushing against it. The fan is activated and without the screen positioned behind the sensor.

exp3 In this scenario, the UAV interact with the sensor by pushing against it. The fan is not activated and with the screen positioned behind the sensor.

exp4 In this scenario, the UAV interact with the sensor by pushing against it. The fan is activated and with the screen positioned behind the sensor.

exp5 In this scenario, the UAV interact with the sensor by pushing against it and sliding along the surface of the sensor in one axis. The fan is activated and with the screen positioned behind the sensor.

The summary of the scenarios can be seen in table 5.1.

Table 5.1: Experiments scenario

Experiments	Fan	Screen
exp1	-	-
exp2	✓	-
exp3	-	✓
exp4	✓	✓
exp5	✓	✓

5.1.5 Source of disturbances

In this part of the report, the sources of disturbances during experiments will be explained. In contrast with the simulation where the disturbances are controllable, during the experiments some of the sources of disturbances are deliberately added while some other are uncontrollable. In this part of the report, each source of the disturbance will be explained. Figure 5.5 can be used as a reference for the disturbance sources.

Figure 5.5: A picture of the experiments which includes sources of disturbances

Fan

A standing fan is added to the experiments. The fan is added to induce a direct wind disturbance. The fan is oriented straight to UAV body with the intention of getting the maximum disturbance from the fan towards the UAV. When the fan is activated, the fan velocity is set to its maximum, which is 3.

Screen

A screen is added behind the sensor plate. It is added to induce an indirect wind disturbance. The goal is to increase the effect of wind disturbance by having an indirect wind from the propeller's thrust which is bounced by the screen. The screen that is used during the experiment is a big whiteboard.

Uncontrollable sources

Uncontrollable sources of disturbances are disturbances which are either inherent to the system or unintentionally added to the system. The possible source of disturbance are listed below

Dangling cable is a bundle of cables which are tethered to a power supply and a PC. This cable added and unpredictable disturbance to the UAV.

Modeling error The wrench observer that is currently implemented in BetaX has a modeling error in it. This is due to the torque control from Pixhawk controller which added another layer of control to the UAV. This additional layer of control has not been included in the wrench observer. This modeling error is affecting the torque part of the wrench observer

5.2 Experiments Results

In this section, the result of the experiment will be presented. This section will be delivered as follow:

First, the observed disturbance will be shown and will be compared against the actual interaction force.

Second, an example of the separation process will be shown.

Third, the result of the separation will be shown and will be compared against the actual interaction force.

5.2.1 Observed disturbance of experiment

The effect of the disturbance towards the wrench observer will be explained in this subsection. The effect of disturbance will be done in one part.

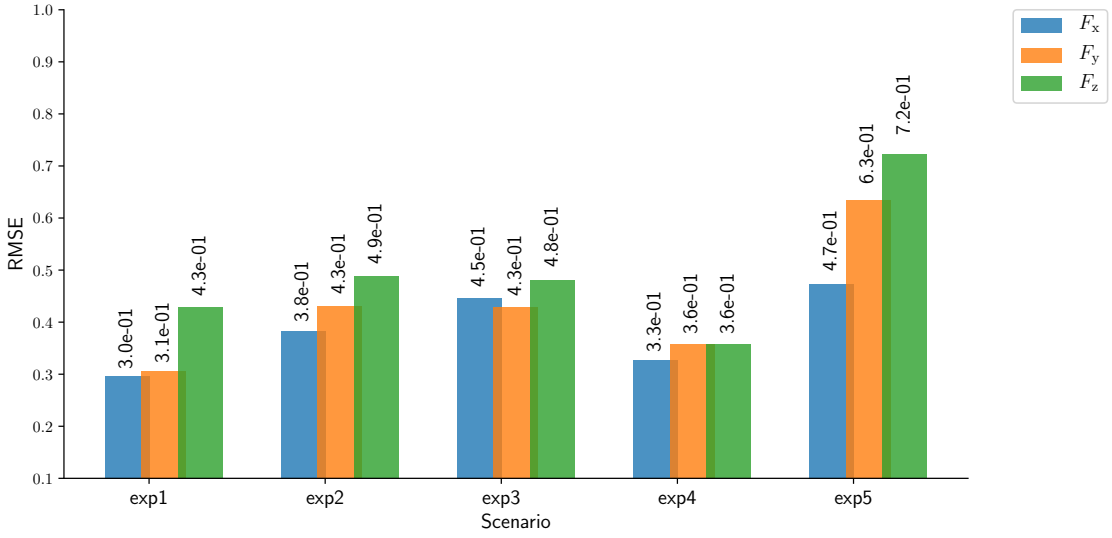

(a) RMSE per-axis

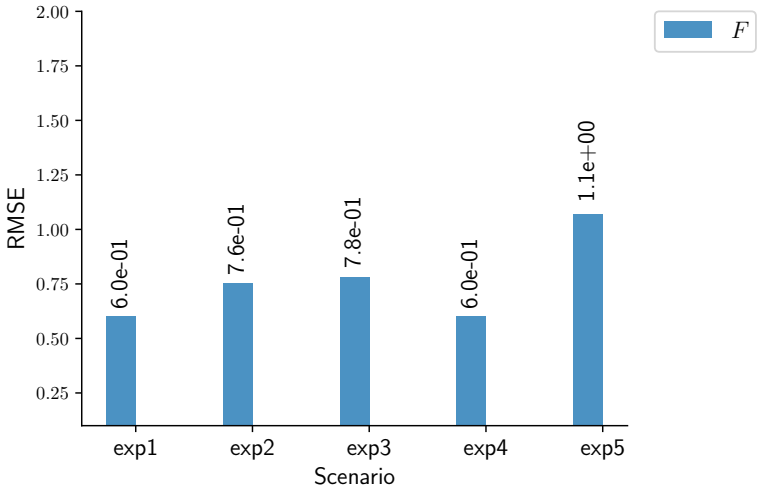

(b) Total RMSE

Figure 5.6: RMSE of disturbance observer F_{obse} against actual interaction F_{inte} with scenarios of different wind orientation

Figure 5.6 shows the RMSE between wrench observer F_{obse} against the ground truth from the torque sensor. By referring to table 5.1, logically, exp4 would have bigger disturbance compare to epx1, epx2, and exp3 since it has the most source of disturbances. However, total RMSE of the scenario shows the contradictory. The total RMSE for exp4 is almost equal to the total disturbance from exp1.

5.2.2 Example of experiment data

In this subsection, an example of the separation process from exp4 will be presented. In this experiment, the fan and the screen will be activated.

Actual position

As explained in the setup of the experiment subsection 5.1.3, the UAV follow a path that is manually controlled. The actual flight path of the UAV is shown in Figure 5.7 and Figure 5.8. The X-axis part of per-axis flight path shows where that the position of the UAV is stopped at around 2.5 where the sensor is located. The 3D plot of the flight path shows how the UAV fly towards the sensor. The detail of the interaction is not visible in this plot.

In Figure 5.7 area which is marked by dashed color can be seen. It represents the assigned separation state. The transition between hovering and calibration is manually assigned by selecting the peak of the disturbance observer during the first collision.

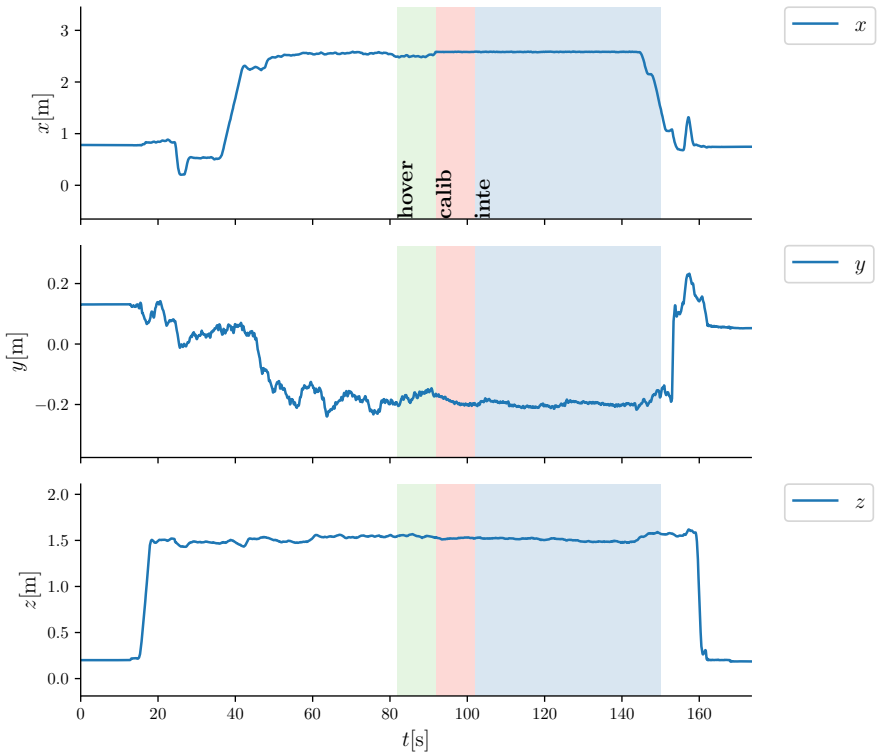

Figure 5.7: Actual path of UAV per-axis. The dashed area color represents the assigned separation state.

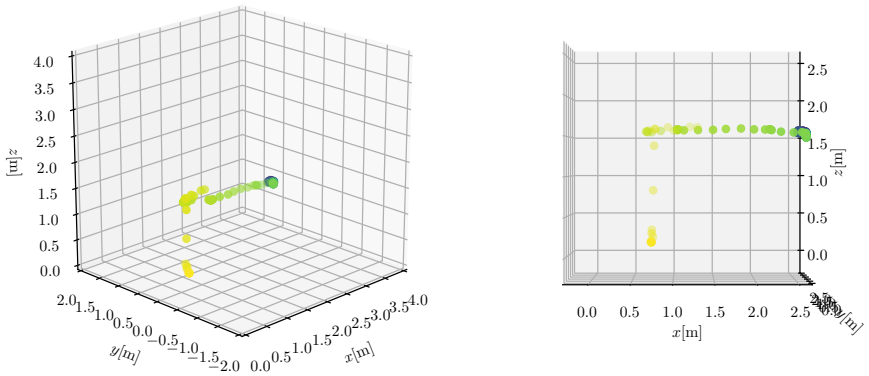

Figure 5.8: Actual path of the UAV in 3D, perspective view (left) and side view (right)

Observed Disturbance

Figure 5.9 shows the observed disturbance compared against ground truth. The figure shows that during the interaction, the error between observed disturbance and the actual interaction, especially in the X-axis, is indistinguishable.

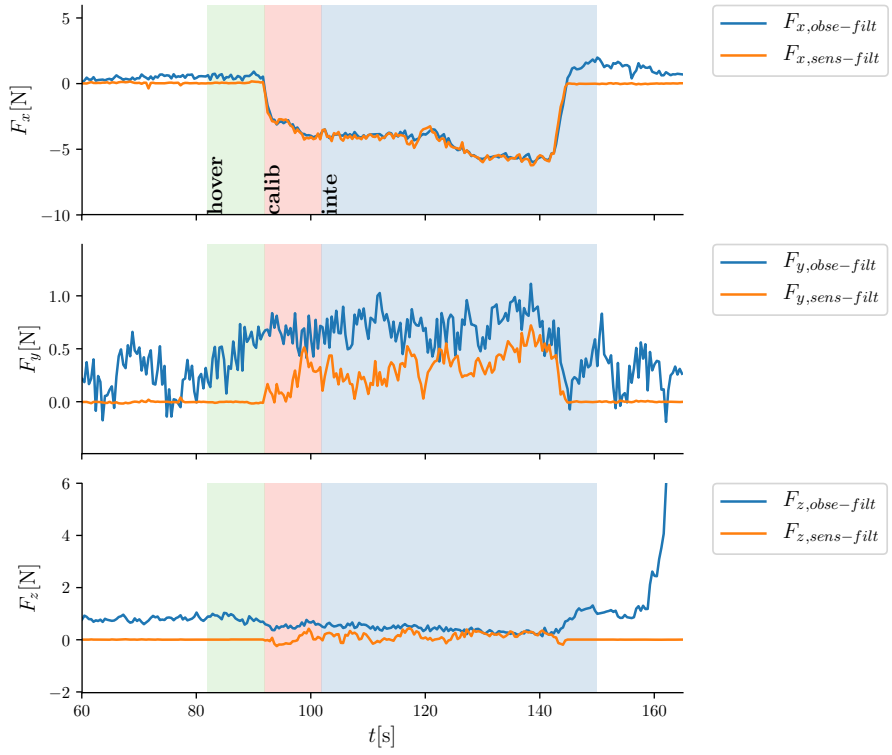

Figure 5.9: Disturbance and interaction component

Unmix observed disturbance using ICA

By fitting the observed disturbance during the calibration state to ICA, the following unmixing matrix A^1 is obtained

$$A^{-1} = \begin{bmatrix} 9.81 \cdot 10^{-2} & 7.91 \cdot 10^{-2} & 4.53 \cdot 10^{-1} \\ -1.81 \cdot 10^{-2} & 4.01 \cdot 10^{-1} & 6.56 \cdot 10^{-1} \\ 6.72 \cdot 10^{-4} & 4.40 \cdot 10^{-1} & -3.12 \cdot 10^{-1} \end{bmatrix} \tag{5.1}$$

Figure 5.10 shows the unmixed independent component (IC) that is transformed from the observed disturbance using the unmixing matrix. From the figure, the component S_1 can be recognized as the interaction component, while the others are not as obvious.

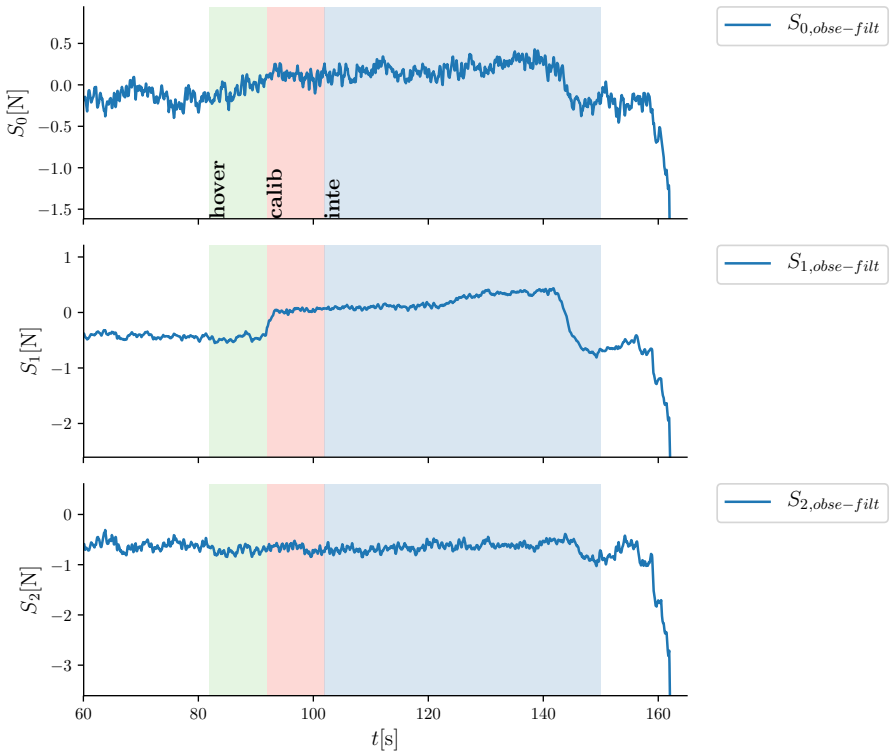

Figure 5.10: Independent component (IC) of disturbance observer

5.2.3 Determine similar IC between hovering and calibration state

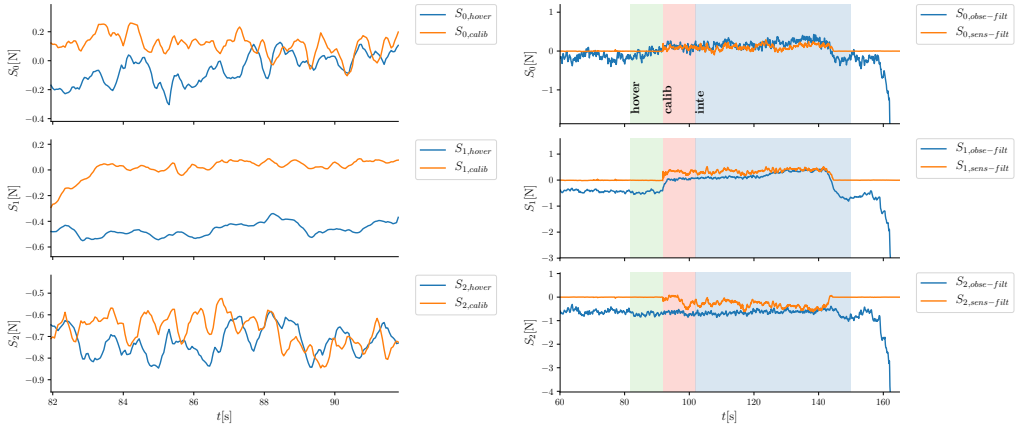

(a) Time domain **(b)** Frequency domain

Figure 5.11: Sampled Independent Components of hover and calibration state.

To determine which component correlate to the disturbance to the disturbance before the interaction, the similarity coefficient is used. The coefficient from the comparing the data in Figure 5.11 is shown below

Table 5.2: Similarity coefficient for each IC

IC	RMS
S_0	$6.86 \cdot 10^{-03}$
S_1	$4.50 \cdot 10^{-02}$
S_2	$5.61 \cdot 10^{-03}$

By looking at the RMS value, it is determined that the IC that is similar between hovering and calibration state is S_2. Using this knowledge and the inverse of the unmixing matrix, a new mixing matrix with the column which correlates to wind disturbance is generated. The filtered-mixing matrix is determined as

$$A_{filt} = \begin{bmatrix} 2.79 \cdot 10^{+0} & -9.29 \cdot 10^{+0} & 0 \\ 1.62 \cdot 10^{+0} & -1.34 \cdot 10^{-1} & 0 \\ -9.13 \cdot 10^{-1} & -1.72 \cdot 10^{-1} & 0 \end{bmatrix}. \tag{5.2}$$

Re-mix the independent component

Using the filtered-mixing matrix, the IC of the observed disturbance is transformed back into its original force space and become the estimated interaction force. The comparison between the estimated force and the actual force is shown in Figure 5.12 while the error plot is shown in Figure 5.13.

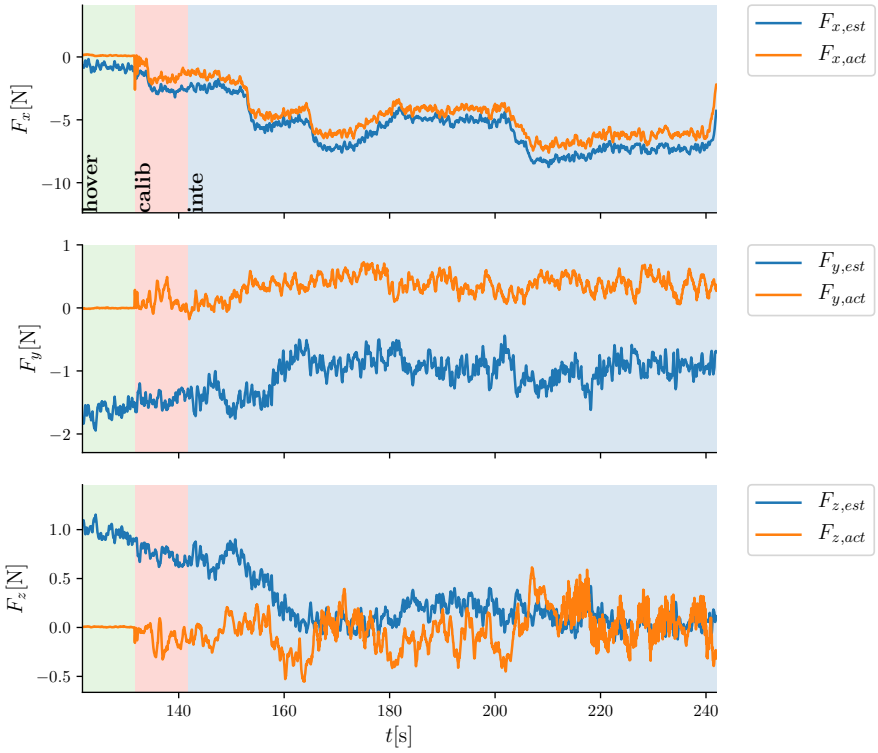

Figure 5.12: Estimated interaction force

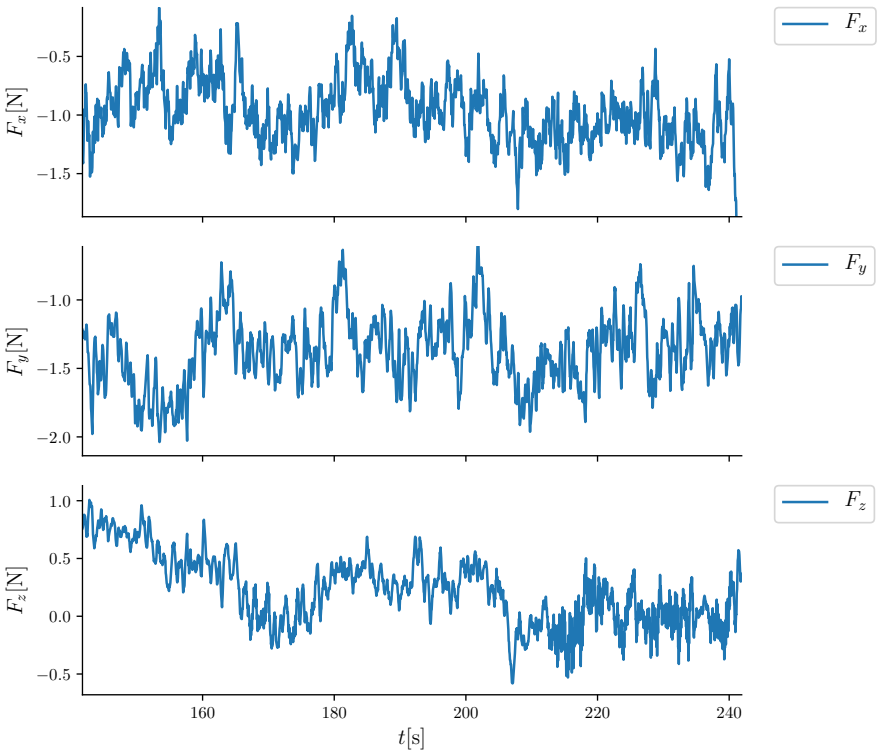

Figure 5.13: Estimated interaction force error

5.2.4 Estimated interaction of experiments

In this subsection, the effect of different scenarios toward the estimation of interaction force through separation will be explained.

Figure 5.14 shows the RMSE between estimated interaction force and the ground truth. It shows that the estimated interaction force have higher RMSE, especially in its X-axis component.

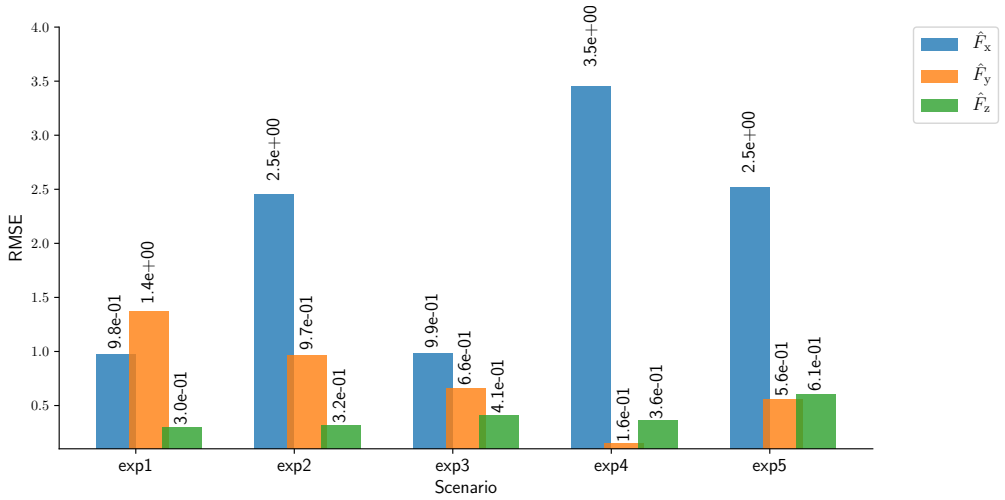

(a) RMSE per axis

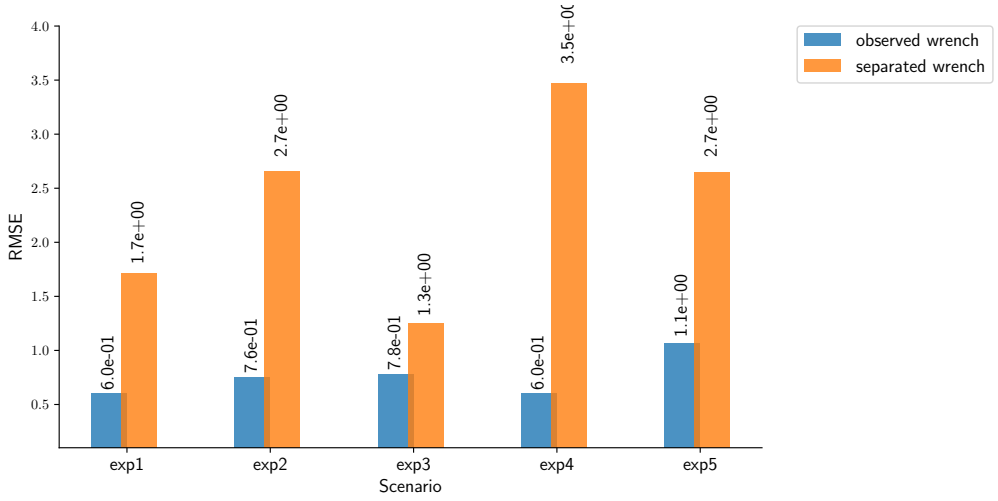

(b) Total RMSE compared with observer data

Figure 5.14: RMSE of estimated interaction force

6 Conclusions and Recommendations

In this chapter, the conclusion from simulation and experiment will be presented including an overall conclusion. Furthermore, some recommendations for future research are also presented.

6.1 Simulation Conclusions

From the result of the simulation, the separation process performs well in scenarios where the source of the disturbance is coming from an orientation that is unique from the orientation of interaction wrench which includes interaction wrench includes friction and contact wrench. It is especially noticeable when the wind is coming from the different direction of either friction or contact wrench. The separation performs well in this case because the columns of the mixing matrix are unique from each other.

In the case of modeling error, the basic ICA method that is used in this thesis is not sufficient to separate it. The problem with modeling error is that the disturbance is not linear.

The method also shows a shortcoming when performed on a scenario without external disturbance. Instead of improving the RMSE of observed force against actual interaction force, it gives worse performance. From looking at the result of the separation, it can be seen that the separated IC is not distinctively independent.

6.2 Experiments Conclusions

Regarding the experimental setups which provide scenarios for wind disturbance, by observing the bar plot of RMSE of disturbance observer against actual interaction, it is apparent that sources of the disturbance are not sufficient to generate observable wind disturbance. The wind disturbance from standing fan and the additional screen which use whiteboard do not provide observable disturbance.

The separation for each scenario in the experiments performed poorly. Instead of improving the estimation of interaction force from the initially observed disturbance, the separation process increases the value of the RMSE. There could be some explanation for the result of the experiment. Other than the same reasons which were provided in simulation conclusions, the environment setup in the experiment added some source of disturbances. Those additional sources include tethering cable and the characteristic of tilted hexarotor—which suffers internal aerodynamic interferences that are complicated to be modeled and cause time-varying disturbances.

Those additional sources of disturbance would make the performance of ICA with only three dimensions of measurement does not perform well in separation.

6.3 Overall Conclusions

Overall, the separation method used in this thesis could perform within some limitation. Those limitations are the limited number of disturbance sources and the assumption that mixing matrix remains static and linear. The number of disturbance is limited by the dimension of observed disturbance which is three in this case. The assumption of static mixing matrix, in this case, is considered to be valid because we use a fully-actuated UAV on a path without changing its orientation.

6.4 Recommendations

To improve the performance of the separation using ICA, issues that can be explored include:

1. Extend the wrench observer, by adding the estimation of propeller thrust and drag model of the UAV to improve the estimation of wrench observer as applied in the work of [9]. It can help the ICA separation because any artifact of independent origin is likely to occupy one degree of freedom in ICA space to model that artifact.

2. Explore the possibility of increasing the dimension of observed disturbance to be able to separate more disturbance sources.

3. Investigate nonlinear ICA to separate nonlinear disturbance, such as modeling error.

4. Explore ICA method which can perform on-line separation to be able to separate disturbance with non-static mixing matrix.

5. From the simulation, it can also be observed that the method to choose similar IC between hovering and calibration state using FFT and RMS is not distinct enough. One improvement that could be implemented in this case is to apply window function before performing FFT to avoid spectral leakage.

6. Finally, the torque part of a wrench needs to be incorporated into the separation, and investigate whether it is possible to combine both component in separation process.

Some recommendations for experiments setups are:

1. BetaX requires a fan, stronger than a standing fan, to have an observable wind disturbance.

2. For disturbance separation, it is better to choose untethered flight to reduce the number of additional disturbance in the UAV.

3. To have a more controlled hover and calibration path, and automatically controlled flight path is preferred.

4. A position marker for the torque sensor also would help in analyzing data from the experiment.

Bibliography

[1] Sangyul Park, Jongbeom Her, Juhyeok Kim, and Dongjun Lee. Design, modeling and control of omni-directional aerial robot. IEEE International Conference on Intelligent Robots and Systems, 2016-Novem:1570–1575, 2016.

[2] Ministry Economy. UAS Flight Operations Levels In the Roadmap for the Application and Technology Development of UAVs in Japan (28th Apr . 2016 The Visual Line of Sight Beyond Visual Line of Sight, 2016.

[3] IEEE ARUAVS. IEEE Aerial Robotics UAVs, 2018.

[4] Rami A Mattar. Development of a Wall-Sticking Drone for Non-Destructive Ultrasonic and Corrosion Testing. Drones, 2(1):8, 2018.

[5] Teodor Tomić, Christian Ott, and Sami Haddadin. External Wrench Estimation, Collision Detection, and Reflex Reaction for Flying Robots, 2017.

[6] M. Fumagalli, R. Naldi, A. MacChelli, R. Carloni, S. Stramigioli, and L. Marconi. Modeling and control of a flying robot for contact inspection. IEEE International Conference on Intelligent Robots and Systems, pages 3532–3537, 2012.

[7] M. H. Raibert and J. J. Craig. Hybrid Position/Force Control of Manipulators. Journal of Dynamic Systems, Measurement, and Control, 103(2):126, 1981.

[8] Teodor Tomić. Evaluation of acceleration-based disturbance observation for multicopter control. In 2014 European Control Conference, ECC 2014, pages 2937–2944, 2014.

[9] Teodor Tomić and Sami Haddadin. Simultaneous estimation of aerodynamic and contact forces in flying robots: Applications to metric wind estimation and collision detection. In Proceedings - IEEE International Conference on Robotics and Automation, volume 2015-June, pages 5290–5296, 2015.

[10] Nicola Diolaiti, Claudio Melchiorri, and Stefano Stramigioli. Contact impedance estimation for robotic systems. IEEE Transactions on Robotics, 21(5):925–935, 2005.

[11] Jonathon Shlens. A Tutorial on Principal Component Analysis. Technical report, Google Research, 2014.

[12] Jonathon Shlens. A Tutorial on Independent Component Analysis. Technical report, Google Research, 2014.

[13] Aapo Hyvärinen, Juha Karhunen, and Erkki Oja. Independent Component Analysis (Adaptive and Learning Systems for Signal Processing, Communications and Control). Wiley, 2001.

[14] Ramy Rashad, Johan B C Engelen, and Stefano Stramigioli. Energy Tank-Based Wrench / Impedance Control of a Fully-Actuated Hexarotor : A Geometric Port-Hamiltonian Approach. submitted to International Conference on Robotics and Automation 2019, 2019.

[15] F Pedregosa, G Varoquaux, A Gramfort, V Michel, B Thirion, O Grisel, M Blondel, P Prettenhofer, R Weiss, V Dubourg, J Vanderplas, A Passos, D Cournapeau, M Brucher, M Perrot, and E Duchesnay. Scikit-learn: Machine Learning in {P}ython. Journal of Machine Learning Research, 12:2825–2830, 2011.